AD-A110 893 NAVAL RESEARCH LAB WASHINGTON DC F/G 20/7
XUV AND XRAY DIAGNOSTICS OF RELATIVISTIC ELECTRON BEAM GENERATE--ETC(U)
FEB 82 R D BLEACH, P G BURKHALTER, D J NAGEL
UNCLASSIFIED NRL-MR-4732 NL

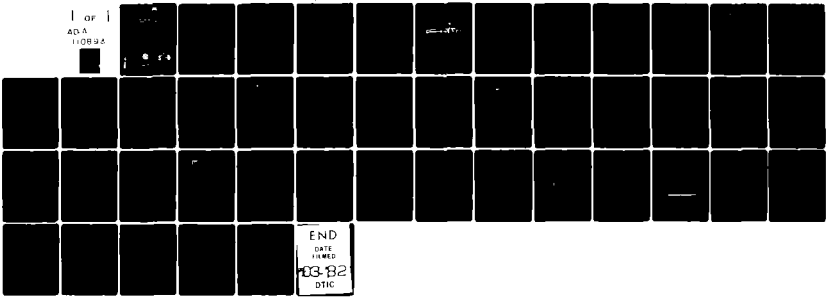

NRL Memorandum Report 4732

XUV and X-Ray Diagnostics of Relativistic Electron Beam Generated Plasmas

R. D. BLEACH, P. G. BURKHALTER, AND D. J. NAGEL

Condensed Matter Physics Branch
Condensed Matter and Radiation Sciences Division

February 8, 1982

This research was sponsored by the Defense Nuclear Agency under Subtask T99QAXLA, work unit 0022, and work unit title, "Satellite X-Ray Simulation Development."

SECURITY CLASSIFICATION OF THIS PAGE (When Data Entered)

REPORT DOCUMENTATION PAGE	READ INSTRUCTIONS BEFORE COMPLETING FORM
1. REPORT NUMBER NRL Memorandum Report 4732	2. GOVT ACCESSION NO. / 3. RECIPIENT'S CATALOG NUMBER
4. TITLE (and Subtitle) XUV AND X-RAY DIAGNOSTICS OF RELATIVISTIC ELECTRON BEAM GENERATED PLASMAS	5. TYPE OF REPORT & PERIOD COVERED Final report — 1978-1980. 6. PERFORMING ORG. REPORT NUMBER
7. AUTHOR(s) R.D. Bleach, P.G. Burkhalter and D.J. Nagel	8. CONTRACT OR GRANT NUMBER(s)
9. PERFORMING ORGANIZATION NAME AND ADDRESS Naval Research Laboratory Washington, DC 20375	10. PROGRAM ELEMENT, PROJECT, TASK AREA & WORK UNIT NUMBERS 62710H; G37MAX/X58; 66H02.60.501
11. CONTROLLING OFFICE NAME AND ADDRESS Defense Nuclear Agency Washington, DC 20305	12. REPORT DATE February 8, 1982 13. NUMBER OF PAGES 45
14. MONITORING AGENCY NAME & ADDRESS(if different from Controlling Office)	15. SECURITY CLASS. (of this report) UNCLASSIFIED 15a. DECLASSIFICATION/DOWNGRADING SCHEDULE

16. DISTRIBUTION STATEMENT (of this Report)

Approved for public release; distribution unlimited.

17. DISTRIBUTION STATEMENT (of the abstract entered in Block 20, if different from Report)

18. SUPPLEMENTARY NOTES

This research was sponsored by the Defense Nuclear Agency under Subtask T99QAXLA, work unit 0022, and work unit title, "Satellite X-Ray Simulation Development."

19. KEY WORDS (Continue on reverse side if necessary and identify by block number)

XUV diagnostics
X-Ray diagnostics
Relativistic electron beams

20. ABSTRACT (Continue on reverse side if necessary and identify by block number)

XUV and x-ray plasma diagnostics were performed on several relativistic electron beam generators. The data yield information on the spectral, temporal and spatial behavior of radiation in the 40 eV-6 keV range for the elements Al, Ti, Cr, Fe, and Ni as well as the noble gases Ne, Ar, Kr, and Xe. Temperatures, electron densities, and emitting volume of the plasmas were determined by direct measurement and comparison with theoretical calculations. These results provide phenomenological data which both characterizes the plasmas empirically and serves to test plasma models.

DD FORM 1 JAN 73 1473 EDITION OF 1 NOV 65 IS OBSOLETE
S/N 0102-014-6601

SECURITY CLASSIFICATION OF THIS PAGE (When Data Entered)

Contents

XUV AND X-RAY DIAGNOSTICS OF RELATIVISTIC ELECTRON BEAM GENERATED PLASMAS

I. INTRODUCTION

Large relativistic electron-beam generators coupled to vacuum diodes can produce dense plasma x-ray sources using different diode loads. Almost a decade ago, single fine wires were shown to be intense x-ray sources[1] in which record ionization stages were observed and identified[2,3] during a systematic exploration of the atomic number dependence of the x-ray emission. Later, the use of imploding-wire-array loads produced plasmas that were larger and more intense than those from single wires.[4] Implosion of hollow gas cylinders formed by puffing gas into the diode immediately before the discharge also produced low-mass, high-temperature plasmas.[5] Plasmas created by the high-power electron discharges, in general, have temperatures exceeding 100 eV and electron densities near 10^{20} cm^{-3}. They emit XUV (10 eV-1 keV) and x-ray (>1 keV) radiation for about 100ns from regions 0.1 to 10 mm in radial extent.

The AURORA generator at Harry Diamond Laboratories, the PITHON generator at Physics International Company, and the BLACKJACK V generator at Maxwell Laboratories were used recently to produce plasmas using gas loads of neon, argon, krypton, and xenon and wire arrays of aluminum and stainless steel. A variety of measurements performed during 1979-1980 in the 2-300 A (40 eV-6 keV) range have been used to characterize the plasmas and are described below. Spectra, time-resolved intensities of the radiation, and images of the emission region have been obtained with spectrographs, spectrometers, and imaging devices. Crystal spectrographs were used to measure K shell spectra from aluminum, argon, and titanium plasmas, and crystal spectrometers were used to obtain time-resolved intensities of argon and titanium K-shell lines. Spatially-resolved L and M shell spectra have been observed in the outer regions of the plasmas with a grazing-incidence grating

Manuscript submitted November 24, 1981.

spectrograph. Time-integrated pinhole and framing camera images, recorded on film, have revealed the size and motion of the plasmas at XUV and x-ray wavelengths. These diagnostic measurements showed that the plasmas are dynamic inhomogenous structures, and an accurate description of them requires resolution of their spectral, temporal and spatial characteristics.

In a previous report,[6] x-ray data from plasmas created by some of the machines cited above was emphasized. In this report, combined spectral, temporal, and spatial measurements in the 40 eV-6 keV range are given. The results of the experiments are grouped according to the generator used. They provide phenomenological data on discharge-heated plasmas which both characterizes the plasmas empirically and serves to test plasma models. A summary of major results is given at the end of the report.

II. INSTRUMENTATION

A. Grazing-Incidence Grating Spectrograph

The grating spectrograph used to obtain time integrated spectra in the 30-300 A range is shown in Figure 1. The instrument is small, which makes it portable and easily adaptable to different generator viewing ports. It was designed and built by the Solar Physics Group at NRL and was used for rocket observations of the Sun. The spectrograph consists of a 10 μm wide entrance slit, a ruled grating, and a film holder all mounted on a 1 m diameter Rowland circle. The grating is ruled at 1200 l/mm and blazed for 1200A in Littrow. This gives an equivalent 128 A blaze wavelength for the 88 degree grazing-incidence angle used. Resolution is about 0.15 A as illustrated by laser-plasma spectrum shown in Figure 2. Higher order spectra are not suppressed, and often second and third order features appear in the spectra. This is a disadvantage when interpreting continuum spectra but aids in identifying line spectra. Spatial resolution was obtained by placing

0.5 mm slit perpendicular to and between the entrance slit and the grating. Kodak 101-01 film was used to record spectra. This film has an uncoated emulsion and requires careful handling. Also, its response to XUV radiation varies from batch to batch making intensity measurements difficult.

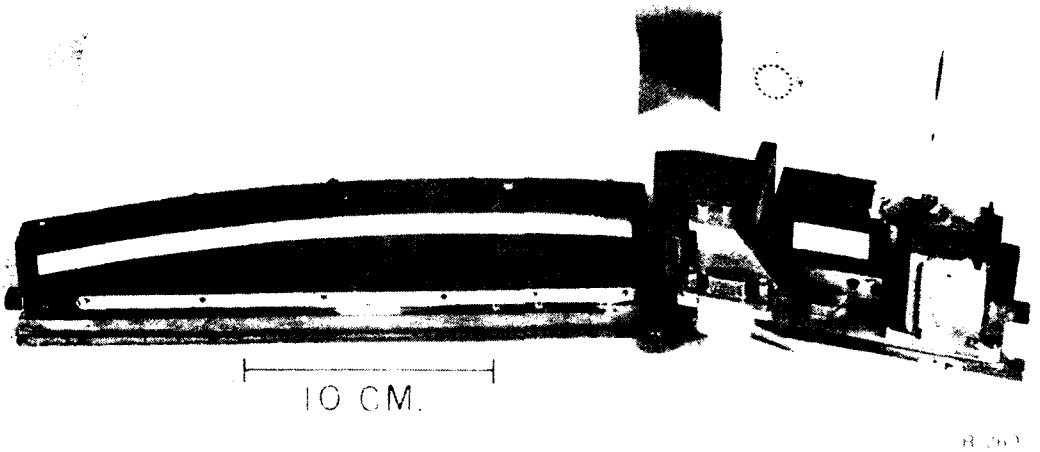

Fig. 1 — A photograph showing the 1 m grating spectrograph used to obtain spectra in the 30-300 A range. The slit (not visible) and grating are on the right, with the long film strip on the left. The housing that covers the spectrograph is also shown in the background.

The spectrograph grating was protected against contamination and damage from hot gases and debris produced in the generator by a fast closure valve which was closed after the radiation was produced but before the gas and debris reached the valve. An air-pressure-driven piston-valve built by the ARACOR Corporation was used for the experiments. The location of the valve is shown in Figure 3. Shutter speeds in the valve are about 10^3 cm/sec producing an aperture closure time of 200 μs. Baffles and transmission screens between the valve and plasma further reduced contamination from accumulating over many shots.

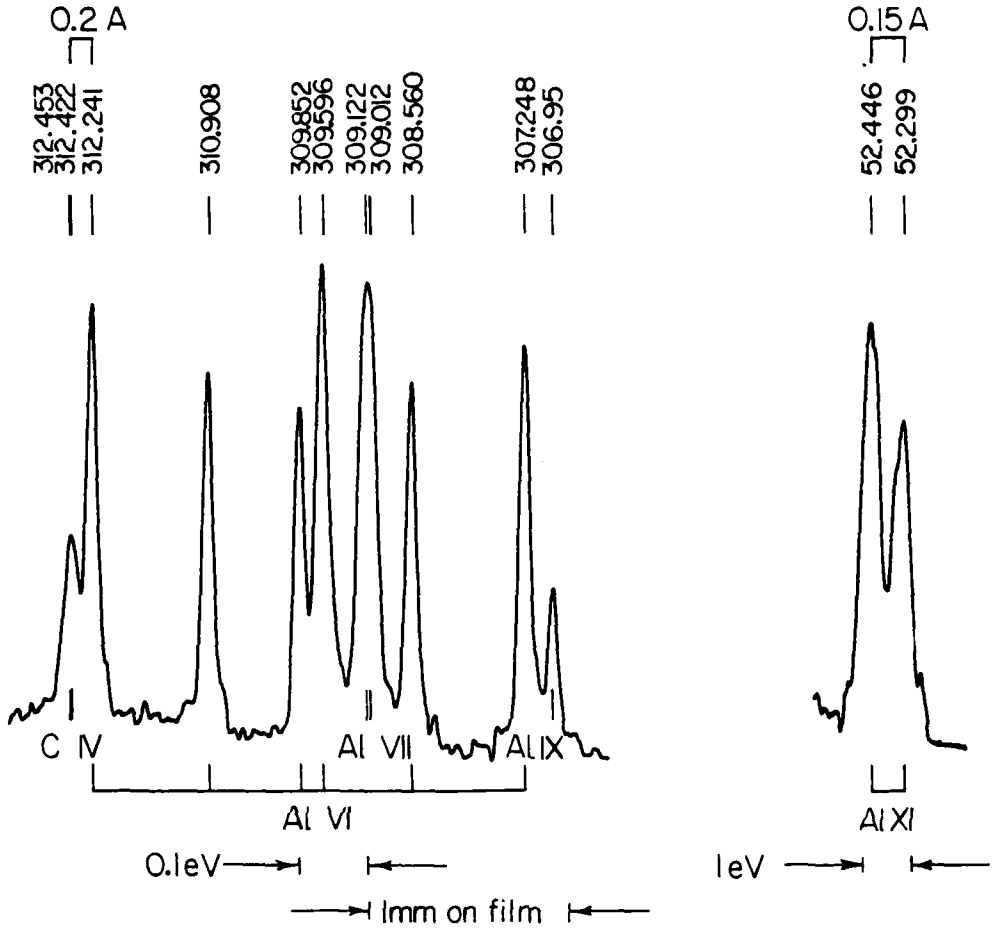

Fig. 2 — Portions of laser-produced Al spectrum obtained with the instrument shown in Fig. 1. Resolution of 0.15 A is measured for wavelengths in the 52-312 A region.

B. Crystal Spectrographs

Convex, curved-crystal spectrographs measured x-ray spectra at energies above 1 keV. These instruments have been previously described[7]. Their major advantage is that a greater wavelength range can be observed through a narrow aperture compared to the same size flat crystal. KAP, LiF, and mica crystals were used depending on the diode load. Spatial resolution was obtained by using a slit in front of the spectrograph. Filters of beryllium and aluminized mylar at the entrance window prevented visible

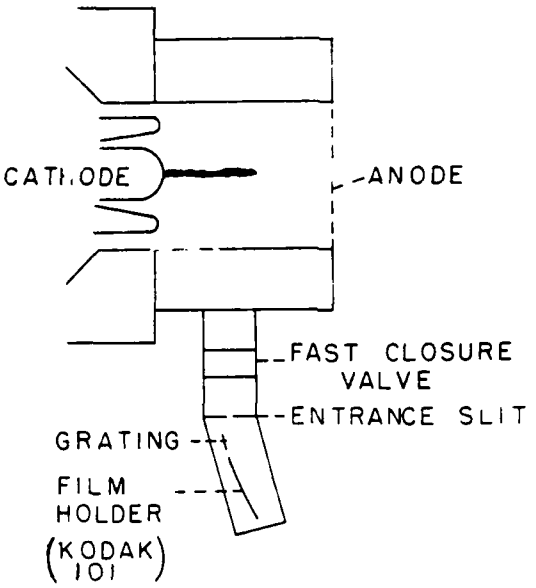

Fig. 3 — A schematic of the experimental set-up used to obtain XUV spectra on the PITHON generator

light from exposing the Kodak No-Screen, Type-T, and Fine-Grain Positive (FGP) films that were used to record the spectra.

A major advance in the use of convex crystal spectrographs occured unexpectedly during the present work. It was found that the (013) planes of KAP diffract Al K lines with both high efficiency and high resolution. Theoretical calculations verified the observed performance and provided quantitative diffraction efficiencies for use in the interpretation of imploded-wire spectra[8]. The computed diffraction efficiency of (001), (002), and (013) planes of KAP is shown in Figure 4, along with data for the (001) plane.

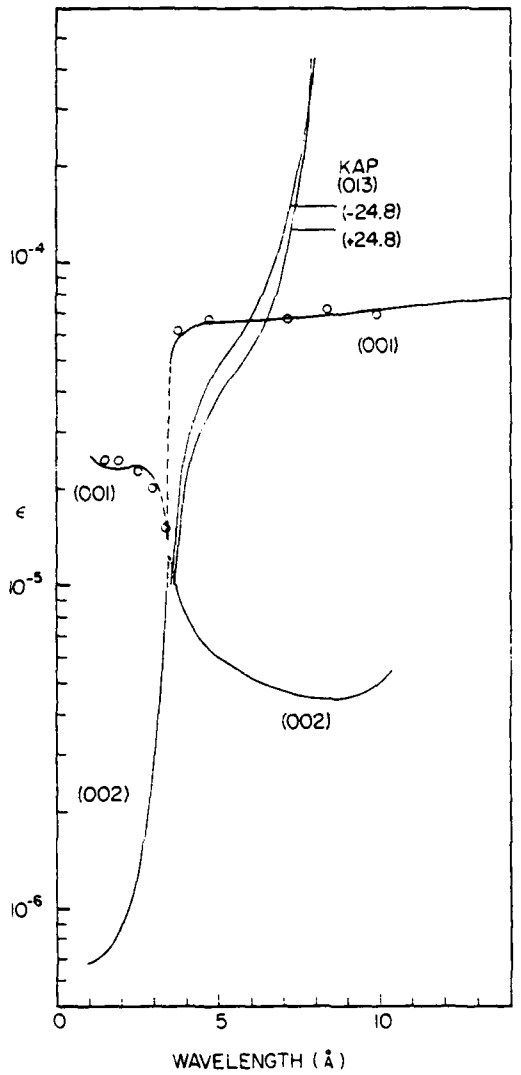

Fig. 4 — Computed wavelength-dependent reflection efficiency for the (001), (002), and (013) planes of KAP (lines), plus measured values (circles)

C. Crystal Spectrometers

Figure 5 shows two schematics of spectrometers constructed with convex crystals and PIN detectors. The top of Figure 5 shows an initial design which uses a convex mica crystal with 2 cm radius of curvature and diffraction from the (003) plane. Two circular PIN detectors each with

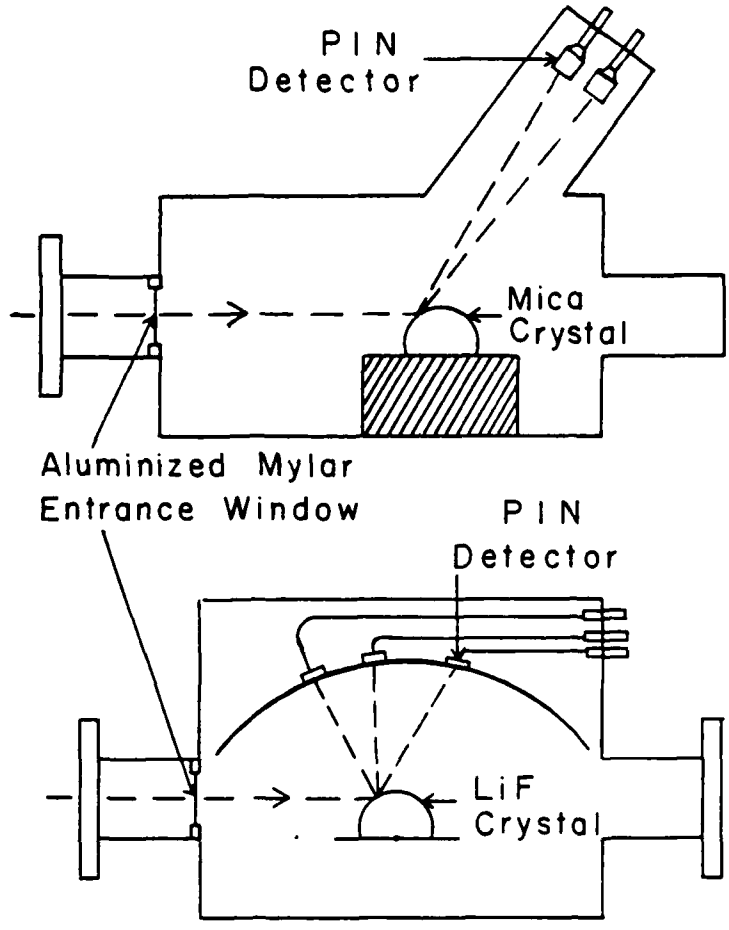

Fig. 5 — Schematics of the crystal spectrometers used to obtain time-resolved x-ray data. The spectrometer shown at the top was used for argon plasmas on the PITHON generator and the spectrometer shown on the bottom was used for titanium plasmas on the BLACKJACK V generator.

a 1 cm diameter and a 15 ns full-width-half-maximum (FWHM) response observed argon H-like 1s-2p and He-like $1s^2$-1s2p lines, one PIN for each line. Each PIN had a 6.4 μm aluminized mylar filter covering it. Initially, a piece of No-Screen x-ray film, which partially obscured the PIN's, was used to determine the correct position for each PIN in order to measure the line of interest.

A second spectrometer, shown schematically at the bottom of Figure 5, used rectangular-shaped (3mm x 12mm) PIN's and a convex LiF crystal to

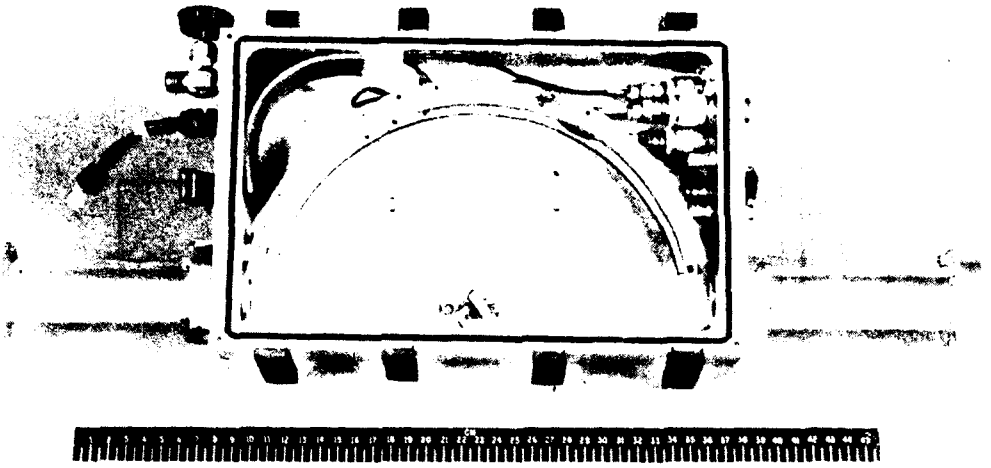

Fig. 6 — A photograph of the LiF crystal spectrometer shown at the bottom of Fig. 5

observe line emission from Ti imploded-wire plasmas. The PIN detectors are mounted on a rail which can be positioned to observe radiation diffracted at different angles. This arrangement provides flexibility to accomodate a variety of crystals and orders of diffraction. A photograph of this instrument is shown in Figure 6. The LiF crystal has a 1.5 cm radius of curvature and diffracts radiation from the (220) plane. H-like 1s-2p and He-like $1s^2$-1s3p lines as well as background radiation were observed from a Ti plasma using three rectangular PIN's at the BLACKJACK V generator at Maxwell Laboratories. Initially, high energy background radiation produced large signals in all the PIN's. It is necessary to reduce this background contamination before line emission can be extracted from the signals.

D. Pinhole Cameras

Pinhole apertures ranging from 50 to 150 μm in diameter were used on most shots. Aluminized mylar filters as thick as 13 μm prevented radiation below about 1 keV from exposing the film. On many shots, different films were stacked behind one another to provide additional attenuation of x-rays. Kodak

No-Screen, Type T, and FGP were used to record the time-integrated x-ray images. The distances between the plasma, pinhole, and film resulted in factors of about 3 in demagnification.

Another method for recording pinhole images was tested on the PITHON generator. A thin layer of aluminum deposited on a 6 μm thick substrate of mylar was used to see if the intense XUV radiation would evaporate the aluminum and produce an image. Previous work on the GAMBLE generator[9] at NRL indicated that soft x-rays evaporated the aluminum while harder radiation was transmitted. Calculations showed that a 1500 A layer of aluminum absorbs most radiation having energy less than 300 eV. An experiment was performed using a 100 μm pinhole in tantalum placed 12 cm in front of a piece of 6 μm thick mylar which was coated with 1500 A of aluminum. The fast closure valve described in section II A was positioned between the argon plasma and the pinhole to prevent hot gases from the plasma from reaching and evaporating the aluminum. After each shot, the aluminum was either not evaporated at all or completely evaporated from the image region depending on the XUV intensity. The lack of intermediate response indicates that the ablation threshold of aluminum is well-defined, and that this method is only useful for obtaining the overall size of the XUV region.

III. EXPERIMENTS AT AURORA

A. X-Ray Spectra

X-ray emission was used to diagnose the imploded-plasma formation in wire experiments with the AURORA generator at Harry Diamond Laboratories. Curved-crystal x-ray spectrographs and pinhole-image cameras were used by personnel from Harry Diamond Laboratories, NRL, and Physics International Company to collect x-ray data from Al and Ti wire array shots at the 6 TW power level. Spectrographs designed at NRL and ARACOR, and pinhole cameras

constructed at HDL and at PI were used to measure temporally and spatially integrated x-ray spectra. Data from several shots were interpreted to obtain plasma parameters. The results are given below. Spectra, recorded on film, were scanned with a Grant densitometer and processed with the film calibrations and computer programs developed at NRL[10,11].

Aluminum spectra were collected in first and second order diffraction from the (001) plane and (013) plane in KAP. Ti spectra were collected using (200) and higher-dispersing (220) planes in LiF crystals. No-Screen and Type T x-ray films were used to record the spectra, and available sensitometric data[10] was used to relate film densities to spectral intensities. The response functions for convex curved LiF and KAP crystals were calculated[12] for the crystals used in these experiments. Spectral resolution is sufficient with the (220) LiF crystals to observe spin-orbit splitting in the Lyman γ line (1s-2p) in Ti XXII. Lyman α line splitting in Al XIII is also observed in KAP (013) plane data.

X-ray spectra were analyzed to determine plasma temperatures and densities. Data from selected shots were scanned with the Grant densitometer using a narrow slit and film densities were measured every 10 μm along the spectra. The densities were digitized and computer processed with a code that corrects for filter absorption, crystal efficiencies, and converts the film densities to intensities. Relative spectral intensities were integrated to obtain line ratios. Temperature estimates in aluminum plasmas were obtained using line ratios of the Hα and Heα resonance lines (Al XIII (1s-2p)/Al XII ($1s^2$-1s2p ^{1}P)) and the Hβ and Heβ lines (Al XIII (1s-3p)/Al XII ($1s^2$-1s5p)). The line ratios depend on the plasma size and the effect of radiation transport in an optically thick plasma. Temperature and density were obtained using line ratios calculated[13] from plasma codes which solved

rate equations in a collisional-radiative equilibrium (CRE) model and compared them with the measured line ratios. Temperatures are listed in Table 1 for four shots with Al arrays and a 750 μm plasma diameter. The ratio of the ^3P to ^1P in Al XII from shot 156 gave a plasma electron density of 1×10^{20} cm^{-3}. A spectral intensity trace of the spectrum recorded on shot 159 is shown in Figure 7. A plasma electron temperature of 630 eV was obtained from the ratio of Hα to Heα lines. This compares with a calculated free-bound continuum temperature of 579 eV. Al plasma temperatures for the AURORA shots are about the same as CRE model temperatures found from Al wire array data taken on other machines at comparable power levels. Figure 8 shows a spectral intensity trace of the first order Al spectrum for shot 169. Resonance lines from Mg impurities in the wires are visible in this spectrum. Close examination of the film revealed Rydberg transitions as high as the 1s-8p line in Al XII.

Table 1
(Top) Temperatures of aluminum plasmas formed on AURORA as calculated from CRE modeling[13].
(Bottom) Temperatures of titanium plasmas formed on AURORA using CRE calculations[13].

ALUMINUM WIRE ARRAYS

Shot	No. Wires	Wire Diam. (μm)	Array Diam. (cm)	Wire Length (cm)	Marx Voltage (kV)	Electron Temp. (eV) Hβ/Heδ	Hα/Heα
156	12	25	2.0	3	90	730	690
158	12	38	2.0	3	100	---	600
159	12	25	2.0	3	100	---	630
169	12	25	1.5	3	100	650	600

TITANIUM WIRE ARRAYS

Shot	No. Wires	Wire Diam. (μm)	Array Diam. (cm)	Wire Length (cm)	Marx Voltage (kV)	Electron Temp. (keV) Hα/Heα
166	12	20	2.5	5	100	2.25
178	12	20	2.0	3	115	2.25
79	12	20	3.0	3	115	1.8

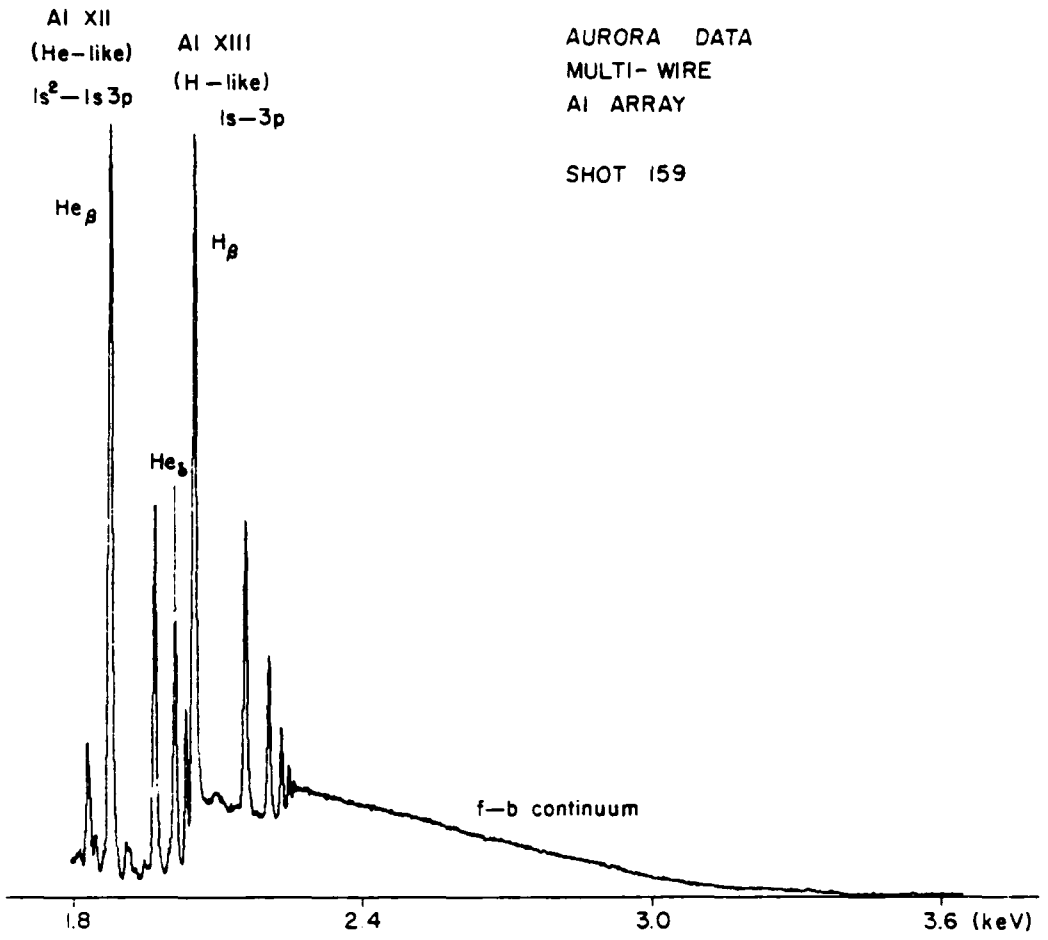

Fig. 7 — The spectral intensity of an aluminum spectrum from AURORA shot 159 obtained with a KAP (001) crystal

X-ray spectral data for Ti wire array shots were analyzed to obtain plasma temperatures. The high quality LiF (200) and (220) crystals were prepared in an earlier DASA-funded program[7]. The entire Ti spectrum for shot 178 obtained with an LiF (220) crystal is shown at the top of Figure 9. An absorption foil, inserted in the spectrograph to cover the portion of the spectrum containing the He-like resonance lines near 2.6 A, prevented over-exposure in this region.

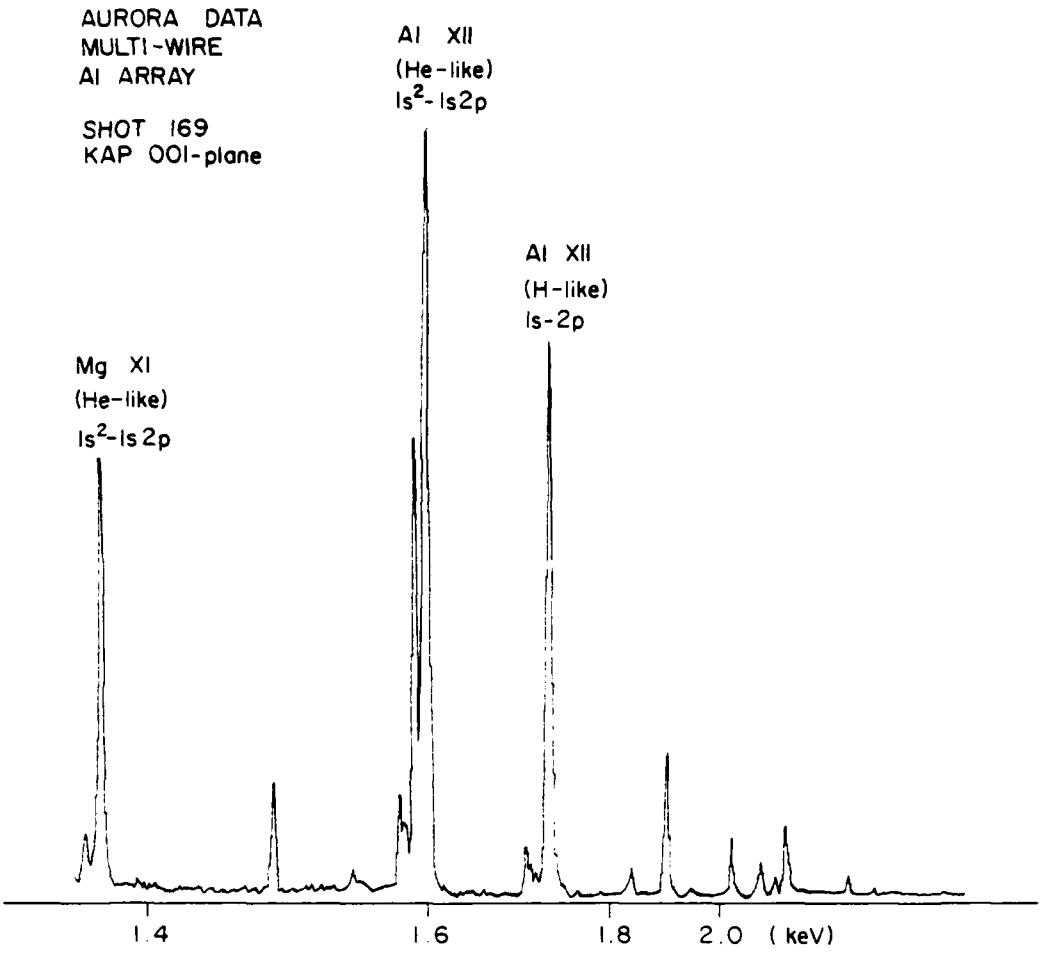

Fig. 8 — The spectral intensity of an aluminum spectrum from AURORA shot 169 obtained with a KAP (001) crystal

The ^1P and ^3P He-like $1s^2$-1s2p lines are about equal in intensity in this shot. Splitting of the Ti XXII 1s-2p lines shows the resolution of the LiF (220) crystal. Ionization stages from Ti X through Ti XXII are observed, but the dominant state is He-like Ti XXI. Plasma temperatures for Ti shots were derived from the Hα to Heα line ratios based on CRE calculations[13] and are given in Table 1. A spectrum from shot 166 using an LiF 200 crystal is shown at the bottom of Figure 9. The plasma electron temperature for this shot was 2.3 keV. A spectral intensity trace of the spectrum from shot 166

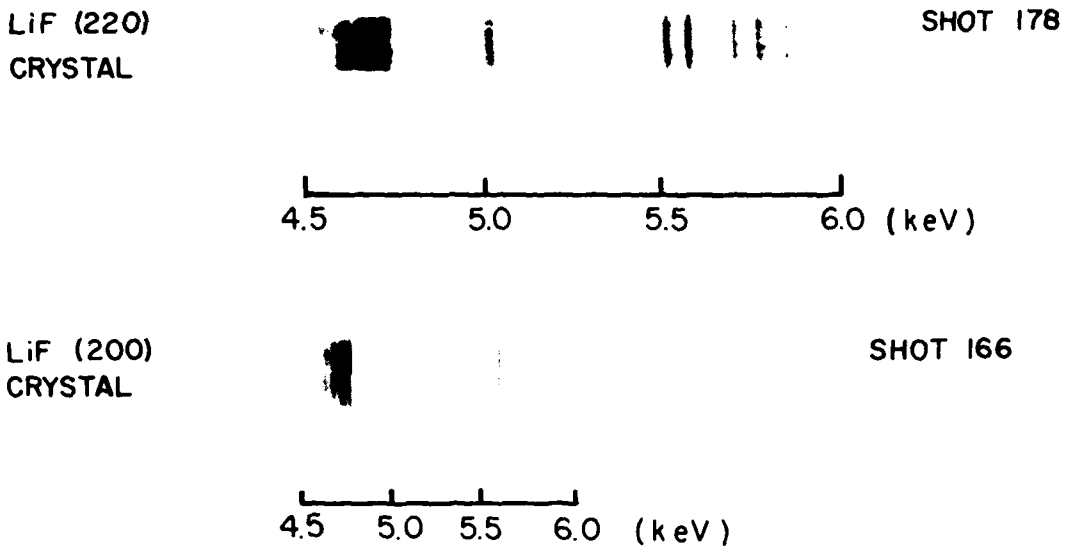

Fig. 9 — Titanium x-ray spectra from AURORA shots 178 (top) and 166 (bottom)

is shown in Figure 10. Intense ^2D satellite lines for the He-like $1s^2$-1s3p and $1s^2$-1s4p lines are observed. Electron densities could not be determined for Ti plasmas since the He-like resonance and intercombination line ratio is not density sensitive at the intensities observed.

B. Pinhole Images of Wire Arrays

Pinhole images for Al and Ti plasmas are shown in Figure 11 for shots 169 and 178. Pinhole sizes ranged from 50 to 150 μm. Aluminized mylar filters 6 μm thick were used to obtain readable exposures for size determinations. In Al plasmas, the intense x-ray emission arises from regions 750 μm in diameter appearing in the image as patches along the axis of the wire array. Ti plasma images consisted of snake-like structures connecting regions of plasma emission that had diameters between 600 and 1200 μm. The images shown in Figure 11 were recorded on Kodak FGP film. They show the non-uniform nature of the plasma implosion. Other images, recorded on Kodak Type T film, which has more sensitivity than FGP, show the implosion core and the outline of the anode which emitted x-rays because of energetic electron bombardment.

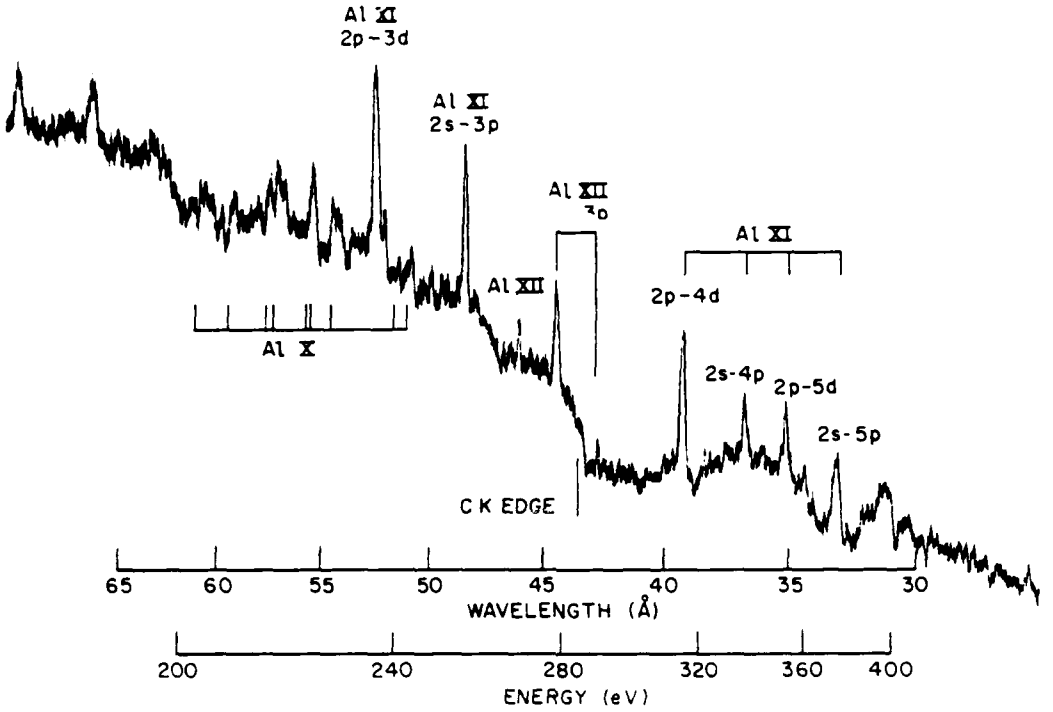

Fig. 12 — A densitometer trace of an aluminum spectrum taken with the grating spectrograph on PITHON shot 846

A. Aluminum Wire Experiments

Figure 12 shows a densitometer trace of a portion of the XUV spectrum of Al from shot 846 taken with the grating spectrograph shown in Figure 1. Twenty-four 25 μm thick Al wires with an array diameter of 1.1 cm were used as the diode load. Spectral lines, formed from a wide range of ionization stages, are superimposed on a continuum consisting of a multitude of line transitions and bremsstrahlung. In the lower energy portion of the spectrum, 2s-2p transitions were identified in Al V-VIII. These identifications were made based on published line tabulations[15]. The dominant lines in the higher energy portion of the spectrum arise from Al XI and can be seen in first, second and third order above the continuum.

In the 200-400 eV region of the spectrum, the most intense lines are from the 2p-3d and 2s-3p transitions in Al XI. A CRE temperature for Al

plasma emission with Al XI lines being dominant is 130 eV. However, the wide range of ionization stages found in the Al plasma, suggest that the XUV emitting region is probably not at a constant temperature. Time histories of the transitions are needed to make more meaningful temperature calculations. Pinhole images of the soft x-ray emission formed by foil burn patterns described in section II D indicate a plasma extending about 1 cm radially from the machine axis.

B. Gas Puff Experiments

Subkilovolt spectra of Ne, Kr, and Xe are described in the following paragraphs, prior to a detailed discussion of the spectral, temporal, and spatial, variation of emission from Ar.

1. Neon

The grating spectrograph was used to take spectra from four shots which varied by a factor of five in machine power. A schematic of the experiment is shown in Figure 3. Figure 13 shows a spectrum from shot 970 which had a relatively high power level. Lines from Ne VII - Ne IX ions (identified by number in Figure 13) were observed on this and the other three shots and are listed in Table 2. At relatively low power, Ne VIII resonance transitions to the 2s level were more intense than excited-state transitions while at high machine power transitions from 3d and 5d levels produced lines more intense than resonance lines. Simple temperature estimates using coronal and L.T.E. models gave electron temperatures in the 50 to 200 eV range.

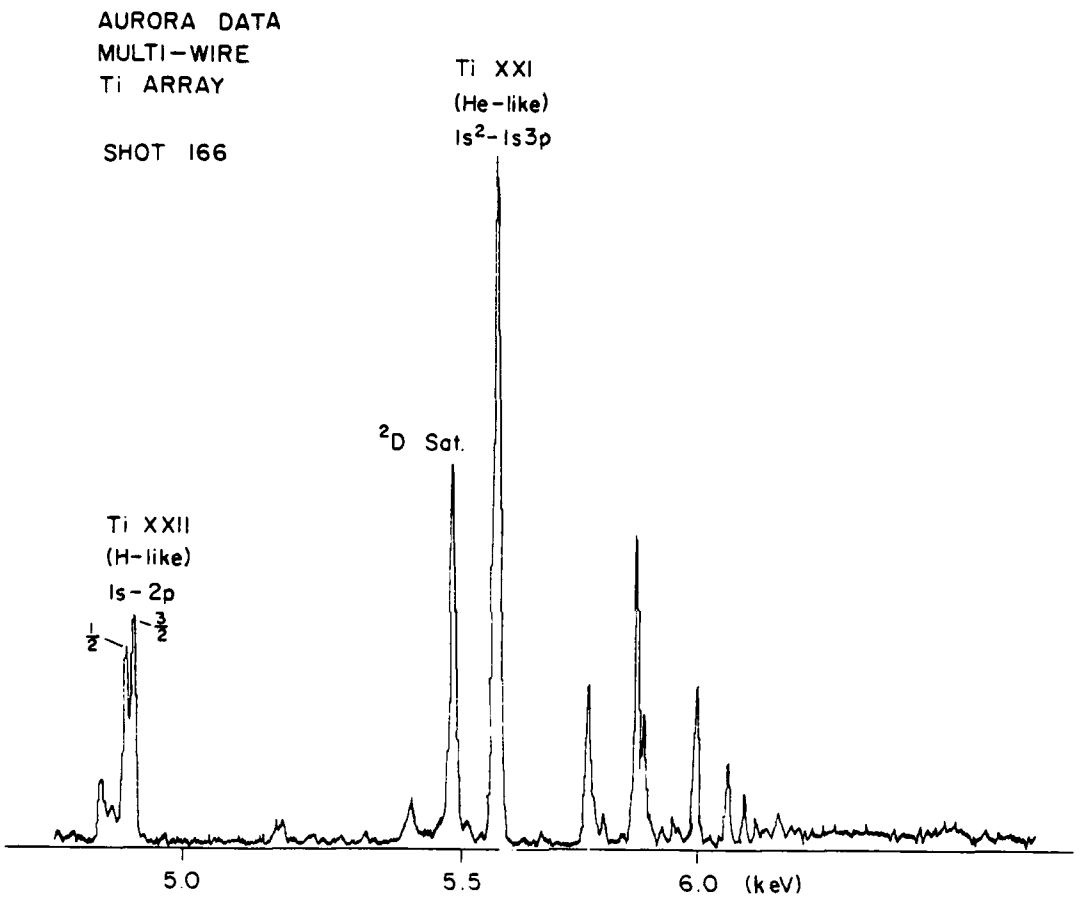

Fig. 10 — The spectral intensity of a titanium spectrum from AURORA shot 166

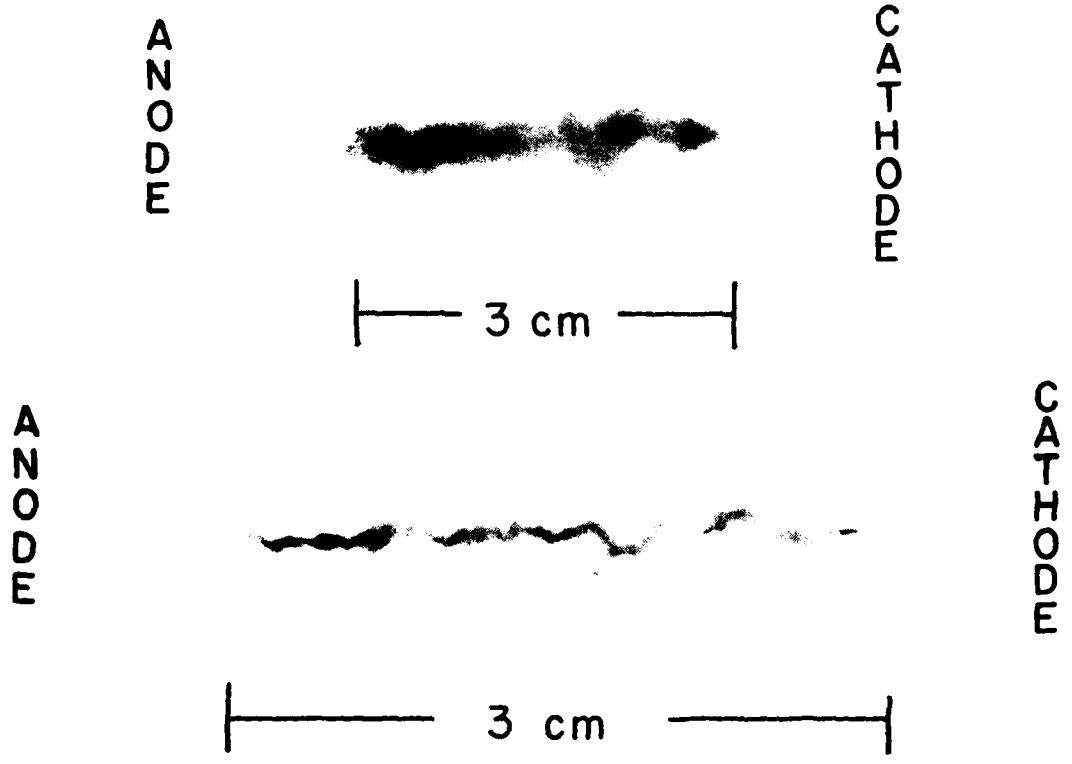

Fig. 11 — X-ray pinhole images of the aluminum plasma taken on AURORA shot 169 (top) and the titanium plasma taken on AURORA shot 178 (bottom)

IV. EXPERIMENTS AT PITHON

X-ray and XUV spectra were observed in aluminum wire array and gas-puff plasmas. X-ray results have been previously reported[14]. The analysis of an aluminum spectrum from shot 846 taken with the grating spectrograph is given below. Gas plasmas of neon, argon, krypton, and xenon were also observed in the x-ray and XUV range. Since most of the shots had an argon gas load, a greater variety of instrumentation measured argon radiation compared to radiation from the other gases. The analysis of argon data follows that of aluminum and the other gas plasmas.

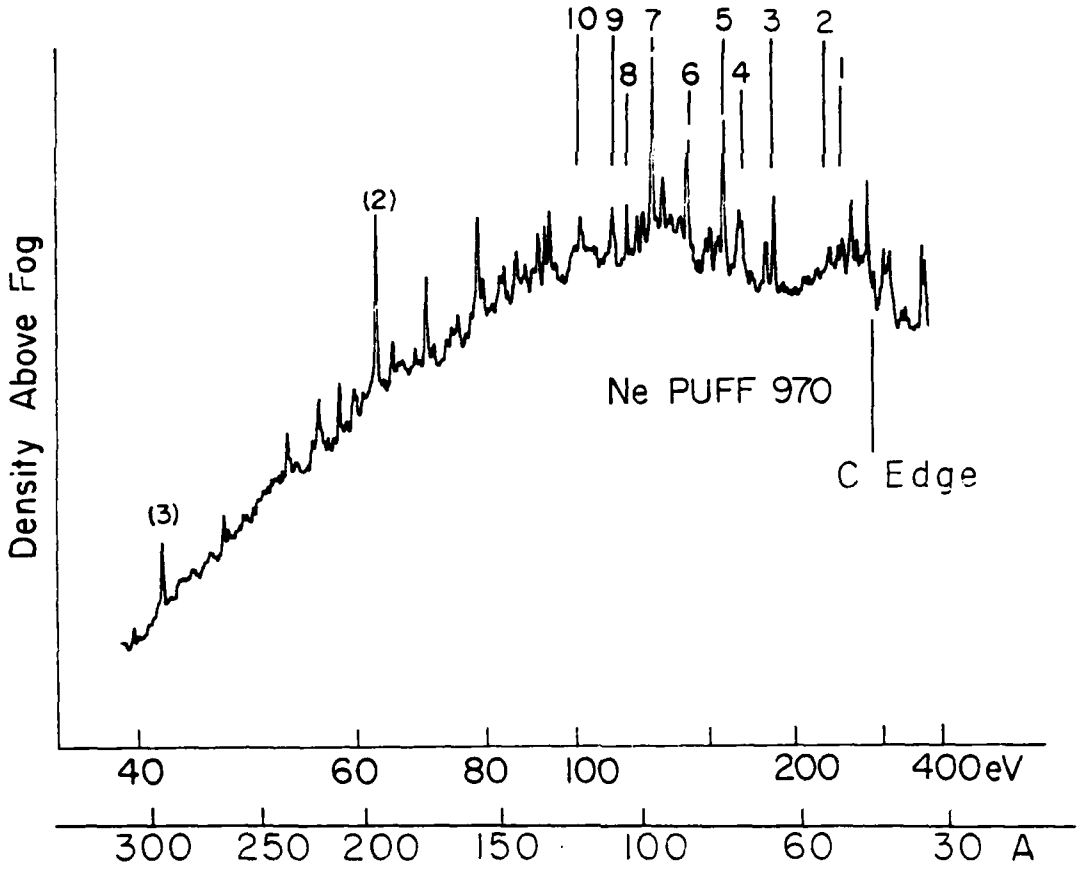

Fig. 13 — A densitometer trace of a neon spectrum from PITHON shot 970 taken with the grating spectrograph. Identifications of numbered lines are given in Table 2.

Table 2
A list of lines appearing in the neon spectrum
shown in Fig. 13 from PITHON shot 970.

Line	Wavelength (A)	Ion	Transition
1	48.0	Ne IX	2p-7d
2	52.4	Ne IX	2p-5d
3	65.8 + 65.9	Ne VIII	2p-5d
4	73.6	Ne VIII	2p-4d
5	78.3	Ne IX	2p-3d
6	88.1	Ne VIII	2s-3p
7	98.1 + 98.3	Ne VIII	2p-3d
8	106.1 + 106.2	Ne VII	2p-3d
9	110.6 + 110.6	Ne VII	2p-3d
10	120.5 + 121.1	Ne VII	2p-3s

(2) and (3) are higher orders of Line 7

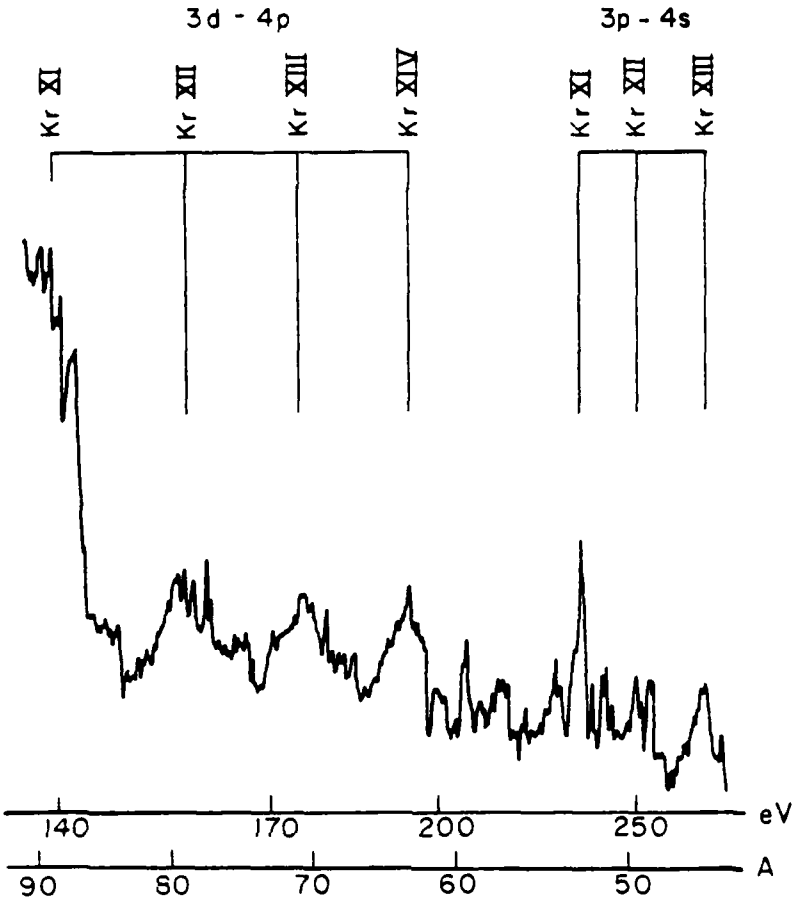

Fig. 14 — A densitometer trace of a portion of a krypton spectrum taken with the grating spectrograph on PITHON shot 964. Identifications of arrays of lines are given in Table 3.

2. Krypton

Dense arrays of lines from Kr X-Kr XII were observed in spectra from two shots. These arrays have been identified[16] as the same seen in spectra of elements with atomic number 37-39.[17] A densitometer trace of a portion of the spectrum from shot 964 is shown in Figure 14.

Arrays were identified by three methods, the results of which are given in Table 3. First, extrapolation of the mean wavelengths and spacings between arrays [17] were within 1 A of the observed centers of gravity. These mean

Table 3
A list of newly-observed transition arrays in the krypton spectrum shown in Fig. 14 from PITHON shot 964.

Ion	Transition	Observed Centers of Gravity Lines (A)	Extrapolation[17] From Lines Previously Observed (A)	Calculated[18] Lines	Calculated[19] Centers of Gravity (A)	
					($np_{3/2}$)	($np_{1/2}$)
Kr XI	3d-4p	89.0	88	88.1*	88.8	89.9
	3p-4s	53.5	--	53.6	52.1	50.5
Kr XII	3d-4p	79.0	79	78.4*	78.7	79.6
	3p-4s	49.5	--	50.1	49.1	47.7
Kr XIII	3d-4p	71.0	71	70.0*	70.5	71.3
	3p-4s	45.5	--	47.1	46.3	45.1
Kr XIV	3d-4p	63.5	--	63.5*	63.5	64.3

* $3d_{5/2} - 4p_{3/2}$ transitions

wavelengths are listed in column 4 of Table 3. Second, a code using a self consistent field method and the Dirac equation provided ground state energy levels of Kr ions.[18] Unfilled levels were also calculated and wavelengths of transitions of interest were within 1.6 A of observed lines. These wavelengths are given in column five of Table 3. Third, a relativistic Hartee-Fock code was used[19] to calculate wavelengths of transitions between centers of gravity of arrays rather than between states of specified L, S, and J. These wavelengths were within 1.4 A of observed lines and are listed in the last two columns of Table 3. The observed ionization stages suggest temperatures in the 50-200 eV range based on coronal and L.T.E. models.

3. Xenon

A densitometer trace of the spectrum from shot 961 obtained with the grating spectrograph is shown in Figure 15. Spectra from four shots show several prominent lines in the 30-60 A range whose wavelengths are listed in Table 4. The lines have not been identified. A coronal equilibrium model[20] suggests that Xe XI and Xe XII dominate the ion population at electron temperatures in the 50-200 eV range. Transitions in Xe XI

and Xe XII ions which produce lines in the 30-60 A range were calculated using an atomic structure code[21].

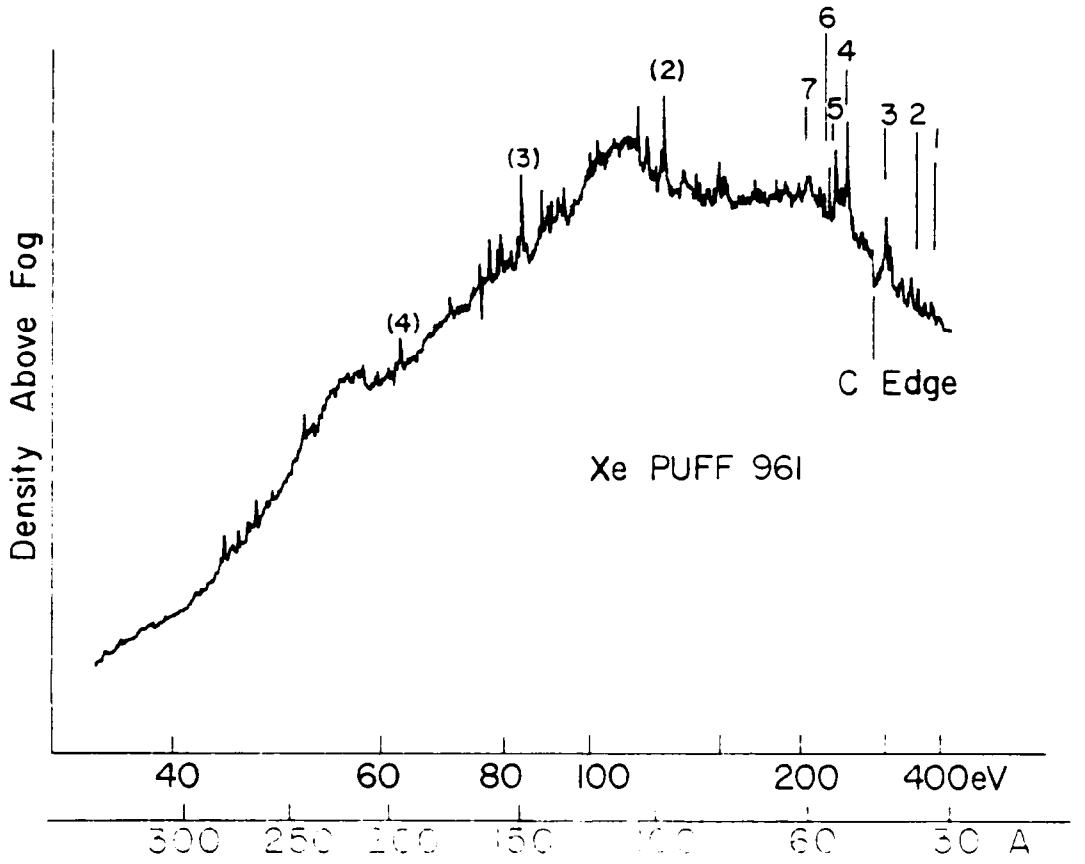

Fig. 15 — A densitometer trace of a xenon spectrum taken with the grating spectrograph on PITHON shot 961. Wavelengths of numbered lines are given in Table 4.

Table 4
Wavelengths of unidentified xenon lines appearing in a spectrum shown in Fig. 15 PITHON shot 961.

Line	Wavelength*(A)
1	32.0
2	34.7
3	41.0
4	49.2
5	51.9
6	53.3
7	58.4

*Measured Wavelengths

(2), (3), and (4) are higher orders of Line 4

No agreement within 0.5 A of the data was obtained. L.T.E. electron temperatures based on Ne line ratios suggest a temperature 2 to 3 times cooler than predicted by the coronal model. At these temperatures the most abundant ionization stages in Xe plasmas are Xe X-XII. Lines from these ions have not been calculated to date.

4. Argon

a. Spatially-Resolved Spectra

On argon shots discussed below, the spectrograph was oriented so that a 500 μm slit gave spatial resolution along the electron propagation axis and viewed a region ± 3 mm perpendicular to the machine axis. The experimental arrangement is similar to that shown schematically in Figure 3. A portion of a spatially-resolved argon spectrum taken on shot 1303 is shown in Figure 16 and a densitometer trace of the spectrum 3 cm from the cathode is shown in Figure 17.

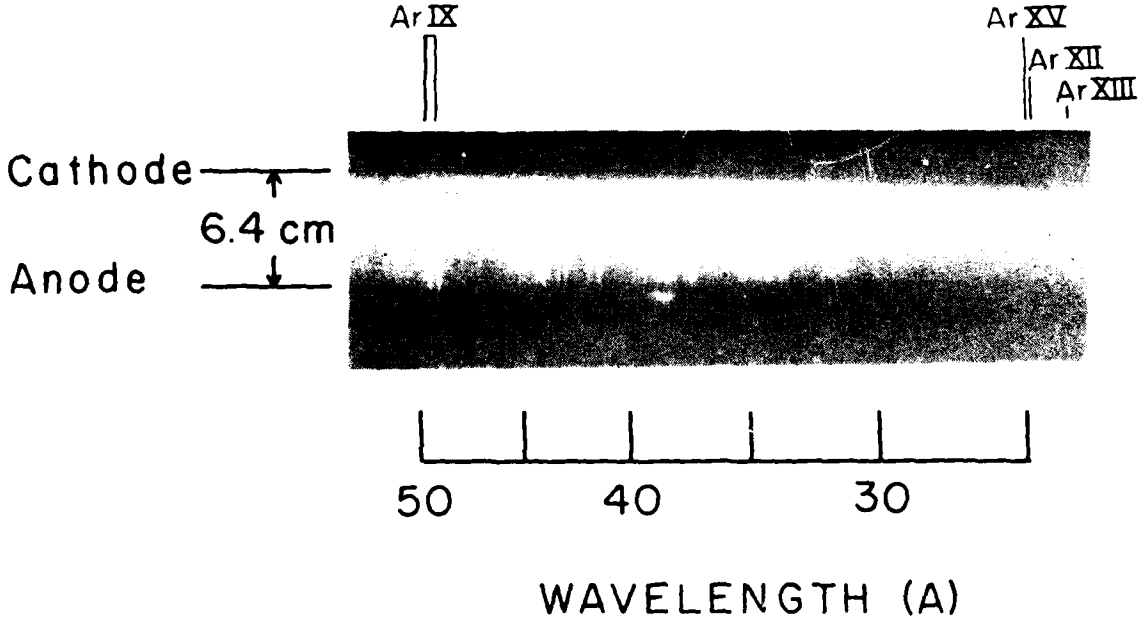

Fig. 16 — A portion of spatially-resolved XUV spectrum of argon from PITHON shot 1303. Lines from higher ionization stages are more intense near the cathode.

Shot 1303 had a measured electrical power of 4.2 TW, a cathode anode spacing of 7.5 cm, and an anode plane composed of stainless steel wire mesh. Spatial resolution of about 0.4 cm along the axis was obtained with the crossed slit. At distances less than about 1 cm from the cathode, lines in the 23-25 A range from Ar XIII-XV ions were observed. As the distance from the cathode increased, these lines rapidly faded in intensity until, at a distance of about 2 cm from the cathode, they were no longer visible. Longer wavelength lines 48.7 A from Ar IX extended from the cathode to about 1 cm beyond the anode plane. In general, lines from the low ionization stages were visible across the cathode-anode space while lines from high ionization stages were stronger near the cathode.

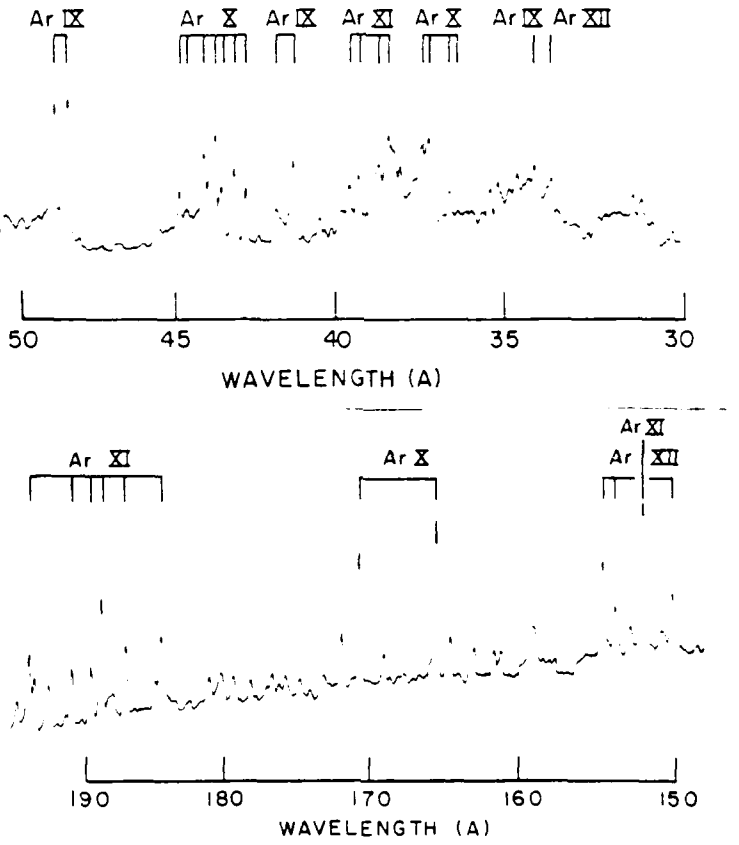

Fig. 17 — A densitometer trace of the Ar spectrum shown in Fig. 16 scanned midway between the cathode and anode on PITHON shot 1303.

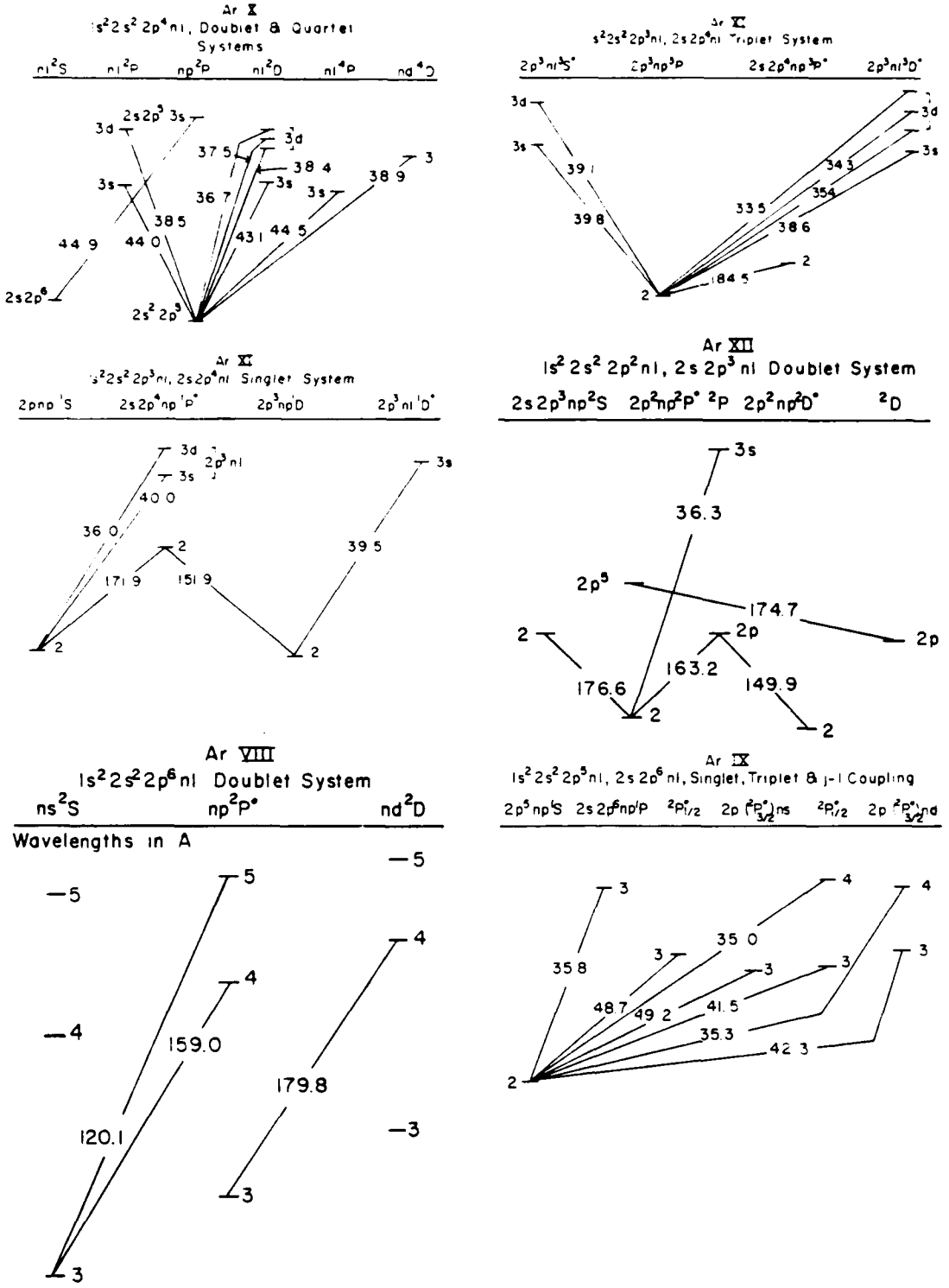

Fig. 18 — Grotrian diagrams showing the Ar VIII, Ar IX, Ar X, Ar XI, and Ar XII lines observed in the PITHON spectra

These results are understood with the aid of time-resolved measurements discussed below. Figure 17 shows a densitometer trace of some of the lines from Ar VIII-XV observed in shot 1303. Figure 18 shows Grotrian diagrams of the observed transitions[22].

Some of the 2s-2p transitions from Ar XI and Ar XII were split into two components which were unequal in intensity and shape. Shot-to-shot differences in the line splittings were observed. Figure 19 shows four densitometer traces of 2s-2p transitions on shots 1280, 1282, 1290, and 1303. The traces were made along a portion of the film corresponding to a distance of 3 cm from the cathode. Line splittings vary between very broad asymmetric components to two relatively narrow symmetric components. The splittings do not correlate with the power ouput of the machine. The highest power shot of the four (1282) produced lines that were broad but not split while lower power shots produced lines that were distinctly split into two components. In the upper left of Figure 19 line splittings spatially resolved midway between the cathode and anode on shot 1281 are shown. The arrow indicates the position of the densitometer scans. The splittings of some lines change from broad unsplit lines near the cathode to two components at the anode.

Separate spectra taken by Lawrence Livermore National Laboratory[23] on PITHON show similar line splittings when viewing the plasma through the anode along the axis of the machine. These observations indicate that Doppler effects are probably not the major cause of the splittings. This differs with conclusions reached by the Lockheed group[24], who observed similar splittings looking perpendicular to the machine axis. A plasma velocity of 2×10^7 cm/sec needed to produce the observed 0.1 eV splittings is consistent with the time in which XUV emission is observed. However, the mechanism of self-reversal can also produce such splittings when viewed

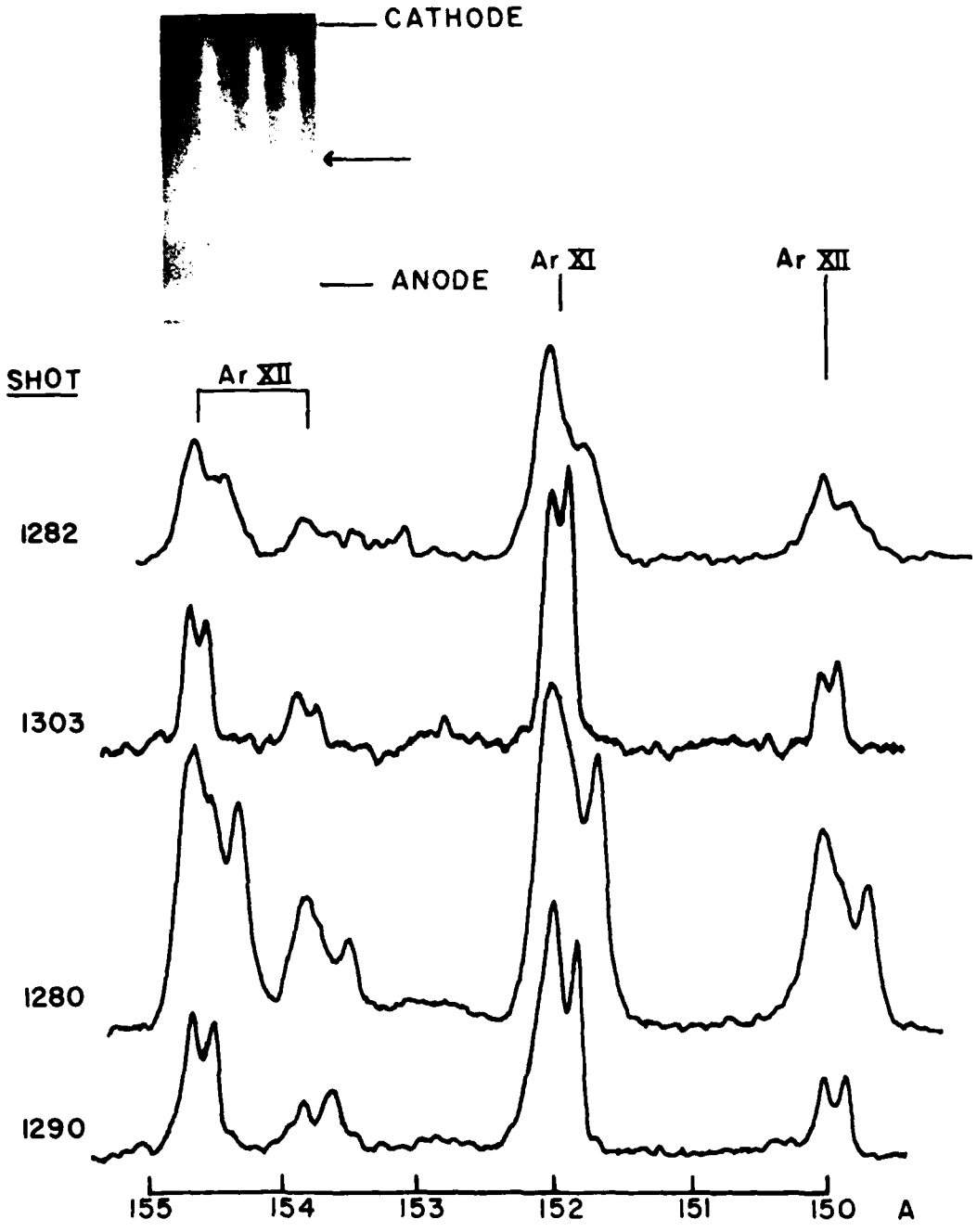

Fig. 19 — Shot-to-shot variations in the splitting and shapes of 2s-2p transitions in Ar spectra. The densitometer traces are identified by PITHON shot number. Shot power increases going from bottom to top. The photographic inset at the upper left shows the corresponding space resolved spectrum from shot 1281 and the arrow marks the position of the densitometer scans on all the spectra.

along and perpendicular to the machine axis whereas the Doppler shift would be observed only when viewed perpendicular to the machine axis. Efforts are underway to predict line shapes and splittings that match the data, but this work is not yet finished. A cool, low density outer region could in theory produce both splitting and asymmetry but the Doppler effects contributing to the line width and asymmetry cannot be ruled out.

The determination of a temperature associated with the plasma is complicated by several factors. First, the plasma is not homogeneous in either space or time. Second, an assumed electron density of about 5×10^{20} cm^{-3} is too low for L.T.E. and too high for coronal equilibrium to be strictly valid. Finally, some of the line radiation is emitted from an optically-thick plasma which can affect line shapes and intensities. Despite these complications, two relatively simple temperature estimates were made. Figure 20 shows a coronal model calculation showing the average ionization stage of argon vs. electron temperature.[20] The most intense argon lines observed are from Ar IX and Ar X. Figure 20 shows that temperatures of 50 to 150 eV are expected. Also, intensities of lines from two adjacent ionization states were ratioed after correcting for line broadening by integration under the line profile and for opacity by a multiplicative factor.

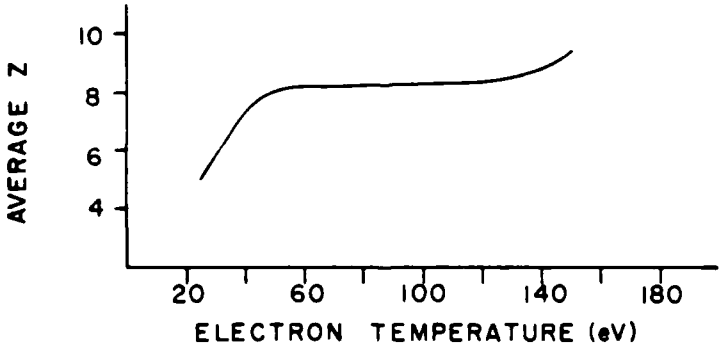

Fig. 20 — A coronal equilibrium model calculation for argon showing the average ionization stage vs. electron temperature[20]

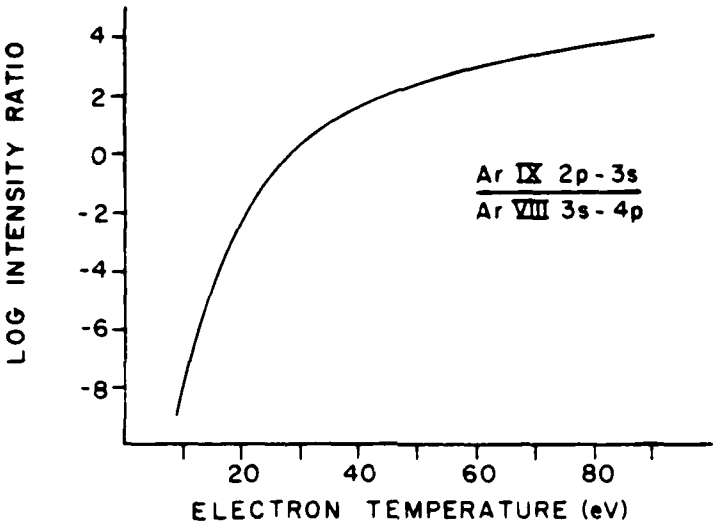

Fig. 21 — A local thermodynamic equilibrium calculation of the ratio of two argon lines vs. electron temperature. The electron density is assumed to be 5×10^{20} cm^{-3}.

An L.T.E. electron temperature of about 40 eV was obtained from Figure 21 using $N_e = 5 \times 10^{20}$ cm^{-3}. This temperature is relatively insensitive to changes in the corrected line ratios. A change in the ratio of two orders of magnitude gives only a 20 eV change in temperature and a change in electron density by a factor of five gives a change in temperature of only 10% at 40 eV.

b. Temporal Variation of Argon Emission

Particles and radiation in the plasmas discussed in this report are usually not in equilibrium with respect to each other during the electron beam pulse. Changes in the plasmas, as previously stated, can be determined by measuring the temporally and spatially-resolved spectra. A time-resolved crystal spectrometer, described in section II C, was to obtain spectra in the 4-6 A range from argon plasmas. Background radiation, measured with an x-ray diode (XRD) outside the spectrometer, was filtered to have about the same energy bandwidth as the PIN's. The data were analyzed to account for different amounts of high energy background detected in the PIN's and XRD on a

given shot. Signals with the same shape as that from the XRD but with amplitude normalized to the film exposure were subtracted as background from the PIN signals. The peak background signal was about 10% of the peak He-like signal. Traces of the PIN signals including background are shown in Figure 22 along with a current monitor trace from shot 1293. The signals are on a relative scale. The ratio of the intensity of the argon resonance lines after background subtraction and the corresponding CRE temperature are also shown in Figure 22.

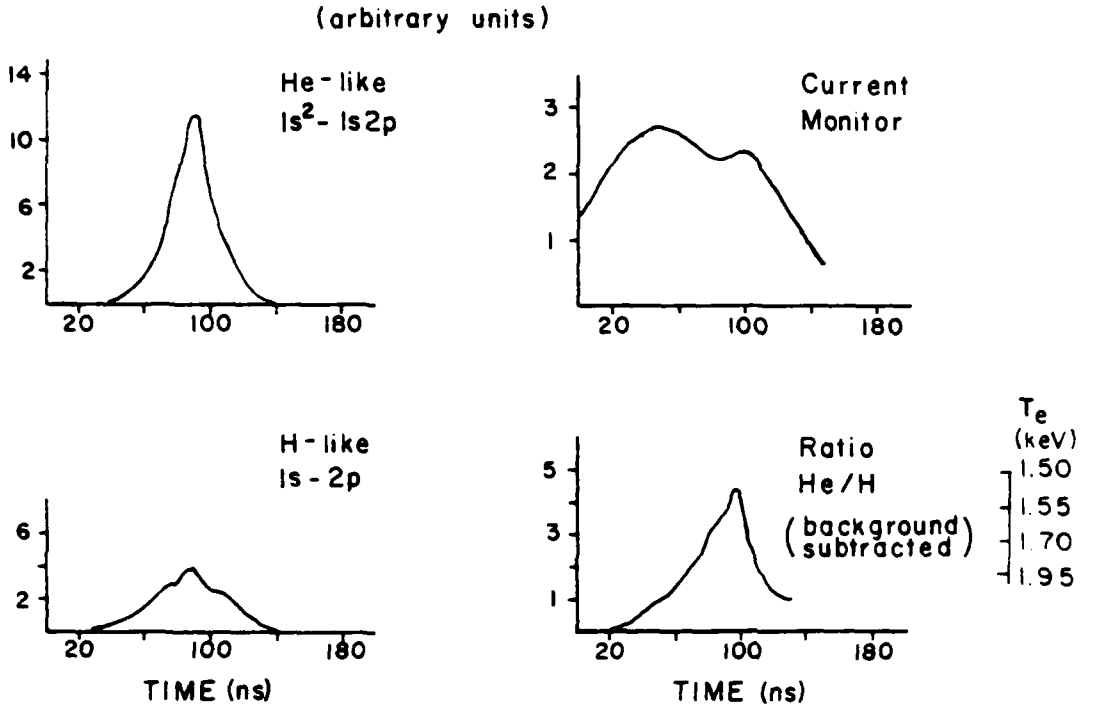

Fig. 22 — Time resolved signals of He and H-like argon resonance lines from PITHON shot 1293 obtained with the spectrometer shown at the top of Fig. 5. A current monitor signal, the He/H line ratio, and the calculated C.R.E. temperature are shown.

The results suggest that the plasma is hotter at the beginning and at the end than in the middle of the discharge. Spatially resolved x-ray spectra and framing camera images taken by Physics International Co. along with the spectrometer results, help explain this result.

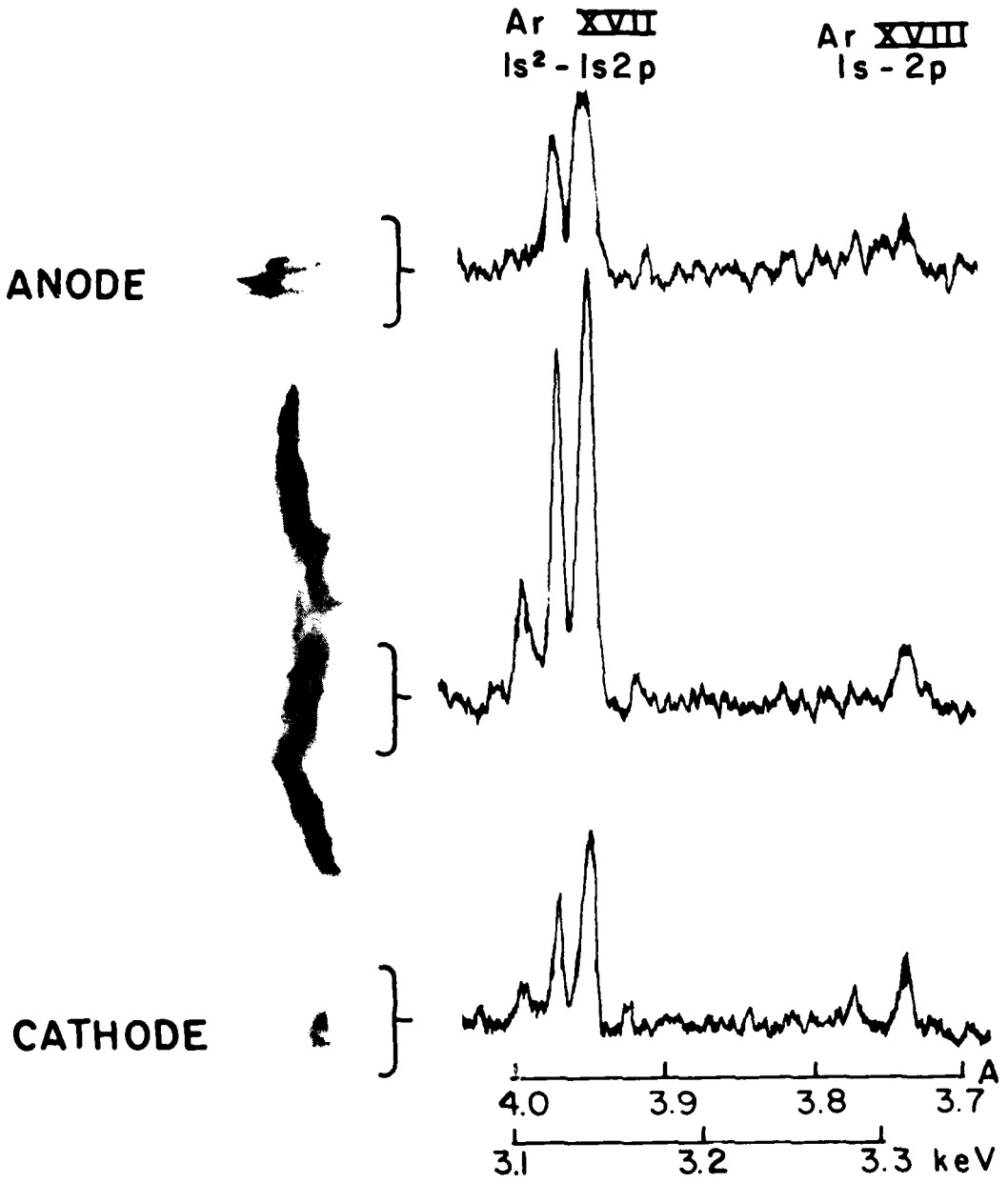

Fig. 23 — Densitometer traces of a spatially-resolved Ar x-ray spectrum corresponding to regions of the plasma in the x-ray pinhole image shown at the left for PITHON shot 1266. The ratio of the He to H-like resonance lines is larger in the center than the cathode or anode sides of the plasma. These data were obtained by R. Schneider of Physics International Co.

Figure 23 shows a densitometer trace of a spatially resolved x-ray spectrum from shot 1264. The He-like line to H-like argon line ratio is smaller at the cathode and anode than between the electrodes suggesting a lower temperature in between than at the cathode and anode. X-ray images, shown in Figure 24, and taken with a microchannel-plate framing camera[25] reveal that, early in time, plasma emission occurs at the cathode(at the left side of each image).

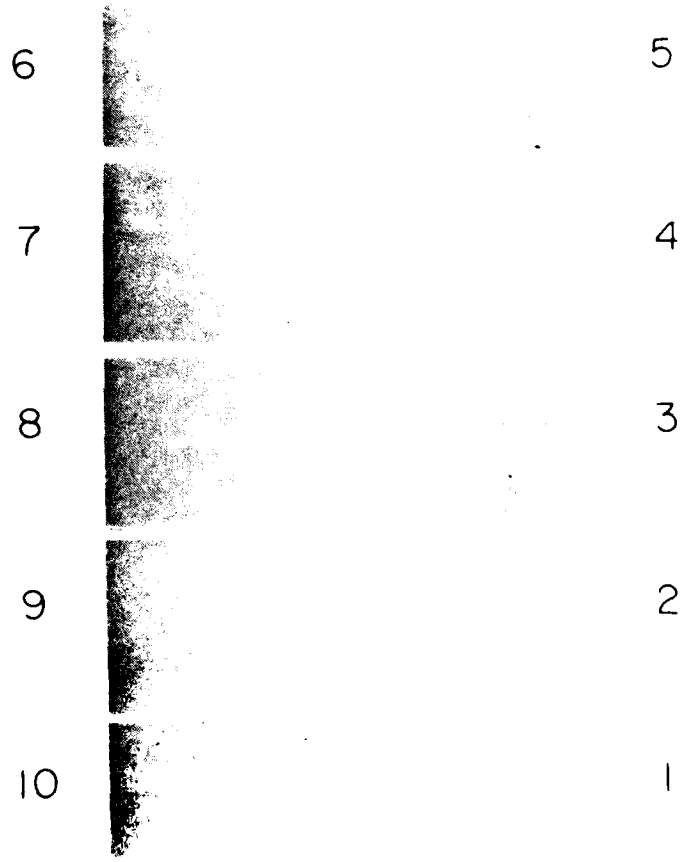

Fig. 24 — A microchannel-plate framing camera sequence of x-ray images showing the propagation of the argon plasmas. The anode side is on the right of each photograph. The duration of each exposure is about 5 ns and the time between exposures is also 5 ns. The framing camera was developed by H. Helava[25] and used by R. Schneider, both of Physics International Co.

The emission propagates towards the anode during the pulse. The results in Figures 22, 23, and 24 show that the changing line ratio obtained with spectrometer is qualitatively explained by the propagating plasma.

C. Spatial Images of Argon Plasmas

The evaporation of aluminized mylar placed in back of a pinhole as described insection II D showed that the XUV emission region was at least 3.6 cm^2 on cross sectional area. Pinhole images on Kodak 101 were also obtained and are shown in Figure 25.

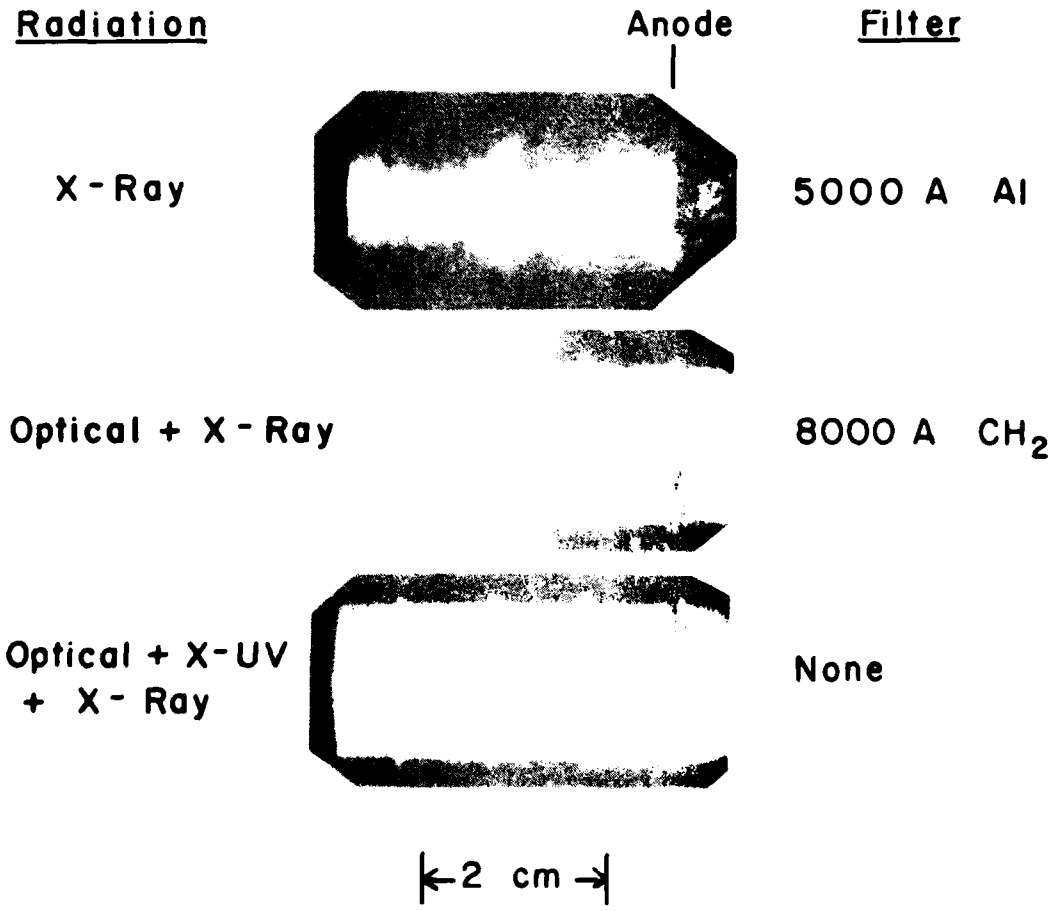

Fig. 25 — Pinhole images of argon plasmas in different wavelength regions selected by filters listed at the right. X-ray emission comes from the inner, hottest region of the plasma.

The top image was made with a 30 μm pinhole and 5000 A of aluminum filtration which allowed transmission of x-rays with energy above 0.5 keV. The center image was made using a 30 μm pinhole and 0.8 μm of polypropylene filtration which allowed transmission of optical radiation and radiation with energies above 0.3 keV. The bottom image was made with a 19 μm pinhole and no filtration. Part of the anode posts on the machine are seen as notches at the top and bottom of each image. The difference in intensity between the bottom and top exposures indicates the emitted optical and XUV radiation. While no quantitative analysis has been done due to lack of calibrated 101 film, the pictures suggest that some XUV radiation is emitted over the entire observed region. Assuming cylindrical symmetry, the observed XUV emitting volume is 4.0 cm^3.

V. EXPERIMENTS AT BLACKJACK

The BLACKJACK V generator at Maxwell Laboratories was used to implode arrays of 12 stainless steel wires each 25 μm thick. Spectra in the 30-300 A range were obtained with two grazing incidence grating spectrographs. The NRL spectrograph is described in section II A. The Maxwell Laboratories spectrograph has a 1200 1/mm ruled grating mounted on a 1 m diameter Rowland circle. Both instruments viewed the plasmas perpendicular to the machine axis. Slits placed perpendicular to the entrance slits of each spectrograph provided spatial resolution. Data were recorded on Kodak 101 film. On a few shots a surface barrier detector placed in the film plane of the Maxwell instrument gave time resolution integrated over the 30-300 A range. Images of the plasma were obtained with pinholes, filters, and film. The carbon filter were 2 μm thick and transmitted radiation in the 44 to 60 A range as well as radiation with wavelengths shorter than 20 A.

A. Spatially and Temporally Resolved Spectra

The spectra recorded on film show discrete line radiation from iron, chromium, and nickel ions superimposed on a background of continuum radiation and blends of lines. A portion of the spectrum on BLACKJACK V shot 956 is shown in Figure 26. Lines from Fe XIV-XIX, Cr XIV-XVIII, and Ni XVII-XVIII were observed and a list is given in Table 5. Wavelengths were obtained from published work [15,26]. The most intense lines in Figure 26 are the 3d-4f transitions noted as Fe XVI radiation. Doublet lines from this Na-like ion are abundant in the spectra. Most of the lines are from transitions between excited states which suggests either a recombining or collisionally-excited plasma. The ratio of the 3d-4f Fe XVI to 3d-4f Fe XV lines gave on L.T.E. electron temperature of 40 eV assuming a 5×10^{19} cm^{-3} electron density.

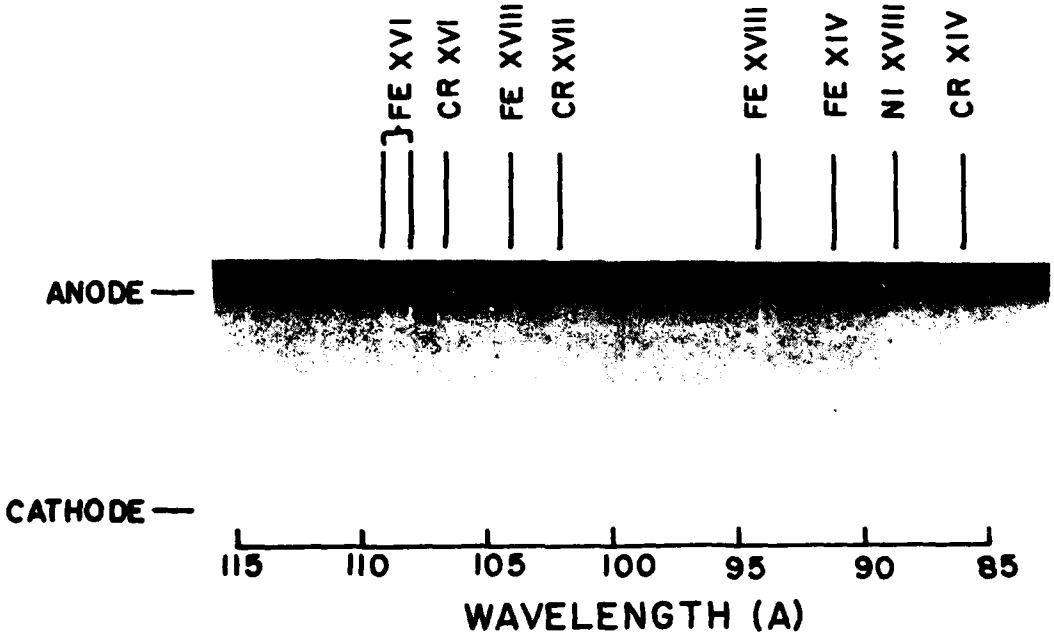

Fig. 26 — A portion of the space-resolved XUV spectrum from BLACKJACK V shot 956. Lines from ionization stages of iron, chromium, and nickel are identified and a complete list is given in Table 5. The cathode-anode separation was 3 cm.

Signals from the surface barrier detector showed that the XUV emission occurs over the entire electrical pulse and peaks midway into the pulse.

Table 5
Lists of observed lines in BLACKJACK V stainless steel spectra.
Wavelengths are in angstroms. See Fig. 26.

Mg-LIKE LINES

Transition	Fe XV	Ni XVII
3p-4d	55.63	55.25
3p-4d	56.20	
3d-4f	69.54	
3d-4f	69.95	
3d-4f	73.47	

Al-LIKE LINES

TRANSITION	Fe XIV
3p-4d	58.96
3d-4p	91.01

Na-LIKE LINES

Transition	Cr XIV	Fe XVI	Ni XVIII
3p-6d		34.86	
3p-6d		35.11	
3s-5p	46.47	36.75	
3d-5p	46.53	36.80	
3d-7f		37.14	
3p-5d	50.81	39.83	32.03
3d-5d	50.16	40.15	32.34
3d-6f		40.20	
3d-6f	52.36	40.25	31.89
3d-5f		40.61	36.99
3d-5f		46.72	37.05
3s-4p	63.31	50.35	41.02
3s-4p	63.53	50.56	42.22
3p-4d	68.57	54.14	43.81
3p-4d	69.18	54.73	44.37
3p-4s		62.88	
3p-4s		63.72	
3p-4f	86.06	66.26	52.62
3d-4f	86.16	66.37	52.72
3d-3d	289.70	251.06	
3p-3d	300.23	262.97	233.79
3s-3p		335.41	292.00
3s-3p			320.56

Table 5.1 (Continued)
List of observed lines in BLACKJACK V stainless steel spectra.
Wavelengths are in angstroms. See Fig. 26.

[illegible] LINES

Transition	[illegible]	[illegible]
2s-2p	[illegible]	[illegible]
2s-2p	[illegible]	[illegible]

[illegible] LINES

Transition	Cr XVII	[illegible]
2s-2p	[illegible]	[illegible]
2s-2p	[illegible]	[illegible]
2s-2p		[illegible]
2s-2p	122.91	[illegible]
2s-2[illegible]	125.36	[illegible]

3-LIKE LINES

Transition	Cr XVIII
2s-2p	104.94

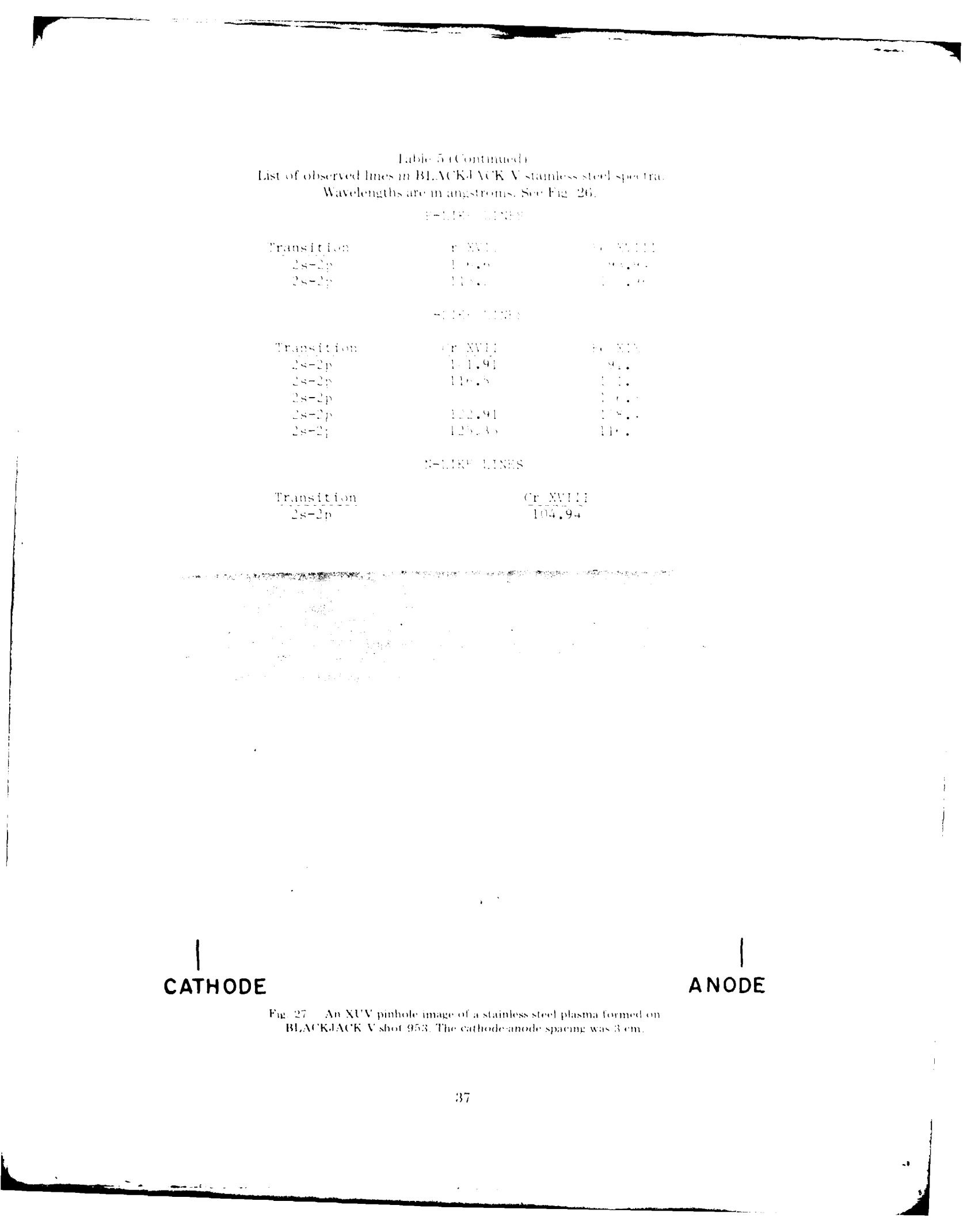

Fig. 27. An XUV pinhole image of a stainless steel plasma formed on BLACKJACK V shot 953. The cathode-anode spacing was 3 cm.

B. Spatial Images

The XUV pinhole image of shot 953 in Figure 27 shows an inner region radiating mostly x-rays above 1 keV and an outer region containing many jets of radiation between 100 and 283 eV. Assuming cylindrical symmetry, the XUV emitting volume is 3 cm^3.

VI. SUMMARY

X-ray data taken on AURORA shots gave electron temperatures in the 600 to 750 eV range from the hottest observed regions in aluminum plasmas and electron densities from these regions of about 10^{20} cm^{-3}. This is the same range of temperatures and densities found in aluminum plasmas formed with other generators at comparable loads and power levels. In contrast, the hottest temperatures found in titanium plasmas are about a factor of three higher than in aluminum plasmas at about equal machine power. Precise electron densities were not determined in titanium plasmas because the resonance to intercombination line ratios are not density sensitive at the measured values. The electron density in titanium plasmas is, however, consistent with 10^{20} cm^{-3}. X-ray emitting regions for both aluminum and titanium plasmas are about 0.6-1.2 mm in radial extent.

The XUV data taken on PITHON showed that aluminum plasma electron temperatures were 4 to 10 times cooler than those found using higher photon energies. Electron densities were not precisely determined but are estimated to be about $5x10^{19}cm^{-3}$ to 10^{20} cm^{-3} by extrapolation from x-ray data. Emitting regions of about 1 cm in radial extent were observed. The PITHON gas-puff plasmas emitting at XUV wavelengths have electron temperatures of about 40 eV. Splittings observed in 2s-2p transitions from Ar XI and Ar XII ions are belived to be predominately caused by self-reversal effects.

Time-histories of argon gas-puff x-ray data have shown that generally a plasma first forms at the cathode and then cools as it propagates towards the anode where it again heats up. This phenomenon may be due to the shape of the gas flow as well as electric field effects at the electrodes.

XUV spectroscopy of stainless steel plasmas produced with the BLACKJACK V generator indicates either a recombining or collisional excited plasma produces the observed line radiation. The bulk of this radiation is coincident with the peak in time of higher energy radiation, and the spatial extent is about 5 times the extent of the emission above 1 keV.

ACKNOWLEDGMENTS

The assistance and advice of K. Kerris and S. Graybill at the AURORA facility, R. Schneider and H. Helava at the PITHON facility, and J. Riordan and J. Pearlman at the BLACKJACK V facility substantially contributed to the gathering and interpretation of the data in this report. We greatly appreciate their efforts. R. Schneider provided Figures 23 and 24 and J. Riordan produced time-resolved XUV data in order to make this report more complete. We thank D. Duston and J. Davis for providing theoretical line intensity ratios which were used to obtain temperature estimated from measured Al and Ti spectra. Information received from Y. Kim (Argonne National Laboratory) and R. Fortner (Lawrence Livermore National Laboratory) is also gratefully acknowledged.

References

1. Mosher, D., Stephanakis, S.J., Vitkovitsky, C.M., Dozier, C.M., Levine, L.S., and Nagel, D.J., Appl. Phys. Lett.,23,419 (1973).

2. Burkhalter, P.G., Dozier C.M., and Nagel D.J., Phys. Rev.,A 15, 700 (1977).

3. Burkhalter, P.G., Dozier, C.M., Stallings, C. and Cowan, R.D., J. Appl. Phys.,49,1092 (1978).

4. Stallings, C., Childers, K., Roth, I. and Schneider, R., Appl. Phys. Lett., 35, 524 (1979).

5. Burkhalter, P.G., Shiloh, J., Fisher, A and Cowan, R.D., J. Appl. Phys., 50, 4532 (1979).

6. Burkhalter, P.G. and Davis, J., Naval Research Laboratory Memorandum Report 3934 (1979).

7. Birks, L.S., Rev. Scient. Instrum, 41, 1129 (1970).

8. Burkhalter, P.G., Brown, D.B., and Gersten, M.J., Appl. Phys.,52, 4379 (1981).

9. Mosher, D. and Nagel, D.J., (Unpublished).

10. Dozier, C.M., Brown, D.B., Birks, L.S., Lyons, P.B. and Benjamin, R.I., J. Appl. Phys., 47, 3732 (1976).

11. Brown, D.B., Criss, J.W. and Birks, L.S., J. Appl. Phys. 47 3722 (1976).

12. Brown, D.B., and Fatemi, M., J. Appl. Phys., 51, 2540 (1980).

13. Duston, D. and Davis, J., Phys. Rev.,A21, 1664 (1980) and private communication.

14. Burkhalter, P.G., Davis, J., Rauch, J., Clark, W., Dahlbacka, G. and Schneider R., J. Appl. Phys.,50, 705 (1979).

15. Kelly, R.L. and Palumbo, L.J., Atomic and Ionic Emission Lines Below 2000 Angstroms, Naval reseach Laboratory Report 7599 (1973).

16. Bleach, R.D., J. Opt. Soc. Am.,70, 861 (1980).

17. Edlén, R., Handb. d. Physik,27,(Berlin, Springer-Verlag), (1964).

18. Liberman, D.A., Waber, J.T. and Comer, D.T., Phys. Rev.,137, A27 (1965).

19. Kim, Y.K., Argonne National Laboratory (private communication, (1979).

20. Breton, C., De Michelis, C., Finkenthal, M., Matholi, M., C.E.A. Report, EVR-CEA-FC-948 (1978).

21. Declaux, J.P., Comp. Phys. Commun.,9, 31 (1975).

22. Bashkin, S. and Stoner, J.O., Atomic Energy Level and Grotrian Diagrams, 2, North Holland Publishing Co., New York (1978) pp. 246-255.

23. Fortner, R. Lawrence Livermore Laboratory (private coomunication, (1980).

24. Perez, J.D., Chase, L.F. McDonald, R.E., Tannenwald, L., and Watson, B. A., J. Appl. Phys.,52, 670 (1981).

25. Helava, H., Eichenberger, C., Gilman, C. and Schneider, R., Bull. of the Amer. Phys. Soc.,24, No. 8 (1979).

26. Mori, K., Otsuka, M. and Kato, T., Atomic Data and Nuc. Tables, 23 196 (1979).

DISTRIBUTION LIST

Director
Defense Nuclear Agency
Washington, DC 20305

Attn: J.Z. Farber (RAEV) — 50 Copies

Maxwell Laboratories, Inc.
9244 Balboa Avenue
San Diego, CA 92123

Attn: J. Pearlman — 1 copy
R.W. Clark — 1 copy
J. Riordan — 1 copy

Naval Research Laboratory

Attn: Code 6680 — 100 copies
Code 2628 — 20 copies
DTIC — 2 copies

Physics International Co.
2700 Merced Street
San Leandro, CA 94577

Attn: R. Schneider — 1 copy
H. Helava — 1 copy

Harry Diamond Laboratories
2800 Powder Mill Road
Adelphi, MD 20783

Attn: S. Graybill — 1 copy
K. Kerris — 1 copy


DATE
FILMED
3-8